Project Number: MQP GSF M102

FORCE SENSING AND HAPTIC FEEDBACK FOR ROBOTIC TELESURGERY

A Major Qualifying Project Report:

Submitted to the Faculty

Of the

WORCESTER POLYTECHNIC INSTITUTE

In partial fulfillment of the requirements for the

Degree of Bachelor of Science

By

____

____

Andrew Marchese

Hubbard Hoyt

Date: April 29th 2010

Approved:

____

Prof. Gregory S. Fischer, Major Advisor

1. Haptics
2. Robotics
3. Robot-Assisted Surgery

TABLE OF CONTENTS

Contents

AUTHORSHIP PAGE

Background Research………. Andrew Marchese, Hubbard Hoyt

Design Alternatives………. Andrew Marchese, Hubbard Hoyt

Final Device………. Andrew Marchese, Hubbard Hoyt

Mechanical Design………. Hubbard Hoyt

Mechanical Implementation………. Hubbard Hoyt

Software Design………. Andrew Marchese

Software Implementation………. Andrew Marchese

Electrical Design………. Andrew Marchese

Electrical Implementation………. Andrew Marchese

ACKNOWLEDGEMENTS

We would like to thank Professor Greg Fischer for his unwavering support during this project as well as committing the resources we needed to make this MQP possible. We would also like to acknowledge all the support and wisdom from the students at WPI AIM lab and CHSL lab, particularly Ivo Dobrev. The team would like to thank Professor Yitzhak Mendelson from the Biomedical Engineering Department at WPI. In addition, we would like to thank the staff and surgeons in the Urology department at Children's Hospital in Boston, in particular Dr. Hiep T. Nguyen and Dr. Brian Minnillo. Without their support and time, we would have not gained such insight on the use and functionality of the *da Vinci* Surgical Robot.

ABSTRACT

Robot-assisted surgery is an alternative to conventional laparoscopic and traditional open surgical techniques. Currently, the primary commercially available robot-assisted surgical system, the *da Vinci* (Intuitive Surgical, Sunnyvale, CA, USA), does not provide haptic feedback to the operator. The goal of this research was to develop a force sensing module capable of integrating with the *da Vinci* surgical system and providing the operator with a representation of end-effecter interaction forces. Additionally, our aim was to develop a system to serve as a test platform for evaluating and implementing haptic feedback and telesurgery techniques. Sensors were developed to measure tool joint torques and calibrated linearly (R^2= 0.99). The sensor module was fit to a *da Vinci* system and physical integration was successful. An industrial robot was retrofitted with a spherical wrist and an embedded Linux control system allowing the attached surgical instrumentation to be articulated about a remote center and emulate *da Vinci* functionality.

TABLE OF FIGURES

TABLE OF TABLES

1. INTRODUCTION

The General Problem

Robot-assisted surgery is a minimally invasive surgical technique in which a slave robot is utilized to manipulate surgical tools. By manipulating a master controller, the surgeon dictates the robot's movements and indirectly the surgical tool's movements. Robot-assisted surgery offers an alternative to conventional laparoscopic procedures where the surgeon directly controls surgical instruments. The *da Vinci* Surgical System (Intuitive Surgical, Sunnyvale, CA, USA) is the primary commercially available system developed for robot-assisted surgery (Intuitive Surgical). This current system is used extensively in urological, gynecological, cardiac, and thoracic procedures. Figure 1 illustrates the typical arrangement of a master-slave robot-assisted surgical system.

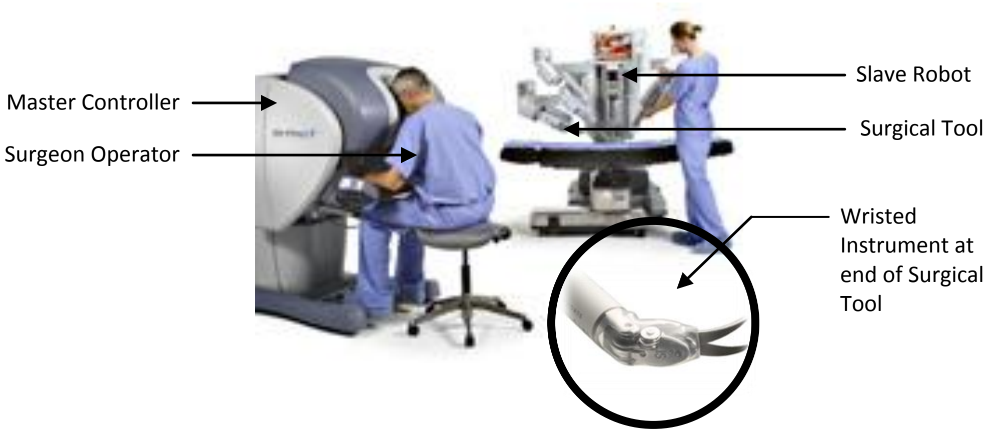

Figure 1.1: Components and layout of master-slave robot-assisted surgery. Specifically, the da Vinci Surgical System is pictured **(Intuitive Surgical)**.

There are several advantages that robot-assisted surgery offers when compared to conventional laparoscopic techniques. The new technique offers increased manipulability and dexterity. The wrist component of the robot-assisted surgical tool allows the operator to achieve seven degrees-of-freedom inside the patient. This is a considerable increase from the four degrees-of-freedom offered to the surgeon during minimally invasive laparoscopic procedures. In the context of ergonomics, conventional laparoscopic procedures require the surgeon to execute awkward and counterintuitive movements as the instrument is pivoted about a fulcrum inverting and constraining tool motion. The master-slave robot-assisted technique allows the operator to intuitively control surgical tool motion. Furthermore, robot-assisted surgery unarguably enhances procedure visualization when compared to conventional laparoscopic techniques. The master console allows the surgeon to see the operating field in three dimensions, restoring the critical element of depth perception found in open surgical techniques (Mottrie) (Elhage, Murphy and Challacombe).

Despite the advantages associated with robot-assisted surgery, the technique presents several disadvantages possibly preventing its assimilation into the operating room and its benefits from being universally enjoyed. For instance, one primary disadvantage of the da Vinci Surgical System is the associate surgical costs. Scales et al. found that robot-assisted prostatectomy (RAP) was only economically competitive with non-robotic radical retropubic prostatectomy (RRP) at high volumes. A very complex cost model is associated with robot-assisted surgery. Besides the initial cost of the system, there are several recurring costs such as maintenance ($100,000 per year), disposable surgical tools ($1,500 per tool), operating room time, and length of stay or hospitalization after the procedure. Because the new procedure's cost is volume dependent, it may not be economically feasible for small and non-specialty hospitals (Scales, Jones and Eisenstein).

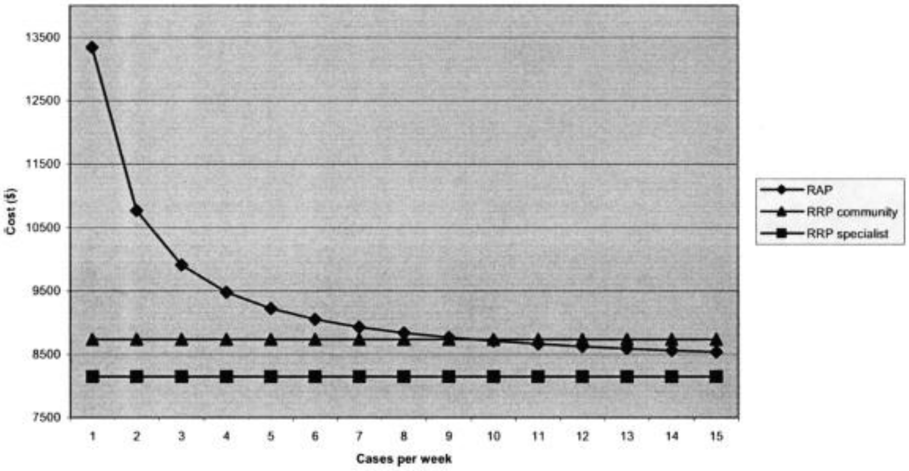

Figure 1.2: Depicts the volume dependency of robot-assisted surgery cost. The robotic technique becomes economically competitive with non-robotic techniques at roughly 10 cases per week (Scales, Jones and Eisenstein).

Furthermore, like any new surgical technique, there is a learning curve associated with robot-assisted surgery. Canadian researchers Lenihan et al. investigated the learning curve of robot-assisted surgery, or the time that it took a surgeon to stabilize operation time while using the *da Vinci* system. The researchers found the learning curve for performing benign gynecological procedures to be fifty operations at ninety-five minutes per operation (Lenihan, Kovanda and Seshadri-Kreaden). The speed at which robot-assisted surgery is incorporated into the operating room may depend on how long it takes operators to become proficient using the new device.

Perhaps one of the most significant shortcomings of robotic-assisted surgery is the absence of haptic feedback, or the surgeon's sensation of tool-interaction forces. Haptic feedback is inherently present in both conventional laparoscopic and traditional open surgery as the surgeon directly manipulates the surgical tools and forces are more easily transmitted through the physical connection. According to Trejos et al., haptic signals can be either kinesthetic, vector forces applied at points or on joints, or tactile, textures and distribution of forces. Haptic cues are an important component of surgery and can enable a surgeon to differentiate tissue, perceive the amount of force applied to tissue, and generally determine the contour and compliance of tissue (Trejos, Jayende and Perri). Many researchers agree that the addition of tactile sensation under proper conditions would be a valuable feature in master-slave robot-assisted surgery (Feller, Lau and Wagner). Tactile feedback typically requires an array of sensors whereas kinesthetic feedback may require the careful placement of very few sensors.

Not only does the absence of haptic feedback prevent a surgeon from exploring the surgical field through touch and relying heavily on visual cues, but it limits the information gathered on the surgical environment. Without a complete picture of the environment, especially tool-tissue interaction forces, a surgeon's judgment and intuition maybe impaired. Furthermore, for advances in robot-assisted procedure where the robot may determine what admissible maneuvers are or apply appropriate safety constraints, a complete picture of the surgical environment is necessary.

Overall Goals

The goal of this design project is to design a device to provide kinesthetic haptic feedback during robot-assisted surgery. Ultimately, the team seeks to develop a force sensing module which seamlessly integrates between a *da Vinci* surgical tool and the robot's arm to measure tool-tissue interaction forces and relay these forces to the operator in an effective manner. Furthermore, this design project aims to develop a test bed for haptics research. It is desired that the platform emulates the functionality of a *da Vinci* arm and articulates a *da Vinci* surgical tool.

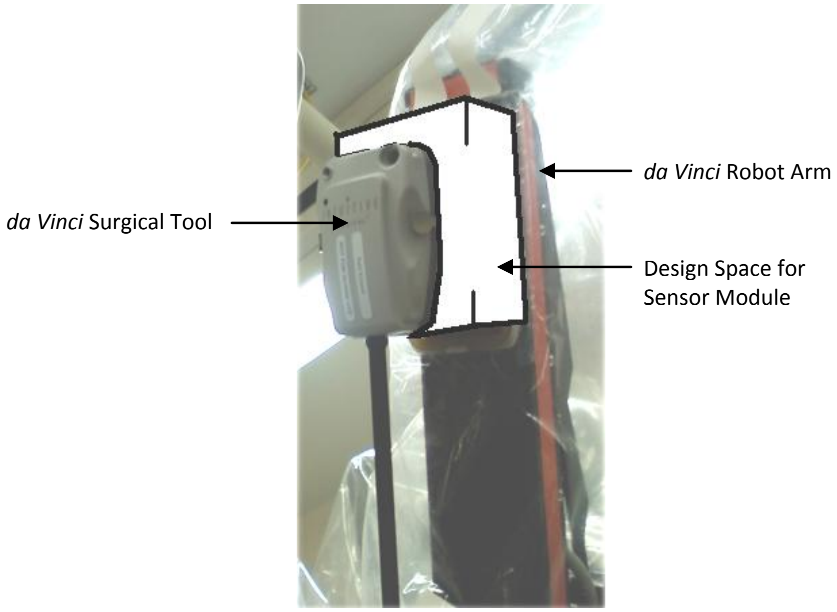

Figure 1.3: The first goal of the design project is to develop a device to measure tool-tissue interaction forces for the purposes of haptic feedback. The goal is for the sensing module to fit between an actual *da Vinci* arm and *da Vinci* surgical tool.

Although the goals of this design project appear to be two separate entities, they are indeed interdependent. Without an actual *da Vinci* system, testing, evaluating and refining a sensor module and haptic feedback device may be extremely difficult. Accordingly, if a research platform is developed in parallel with the sensing module, the platform can ultimately be used to evaluate the sensing device independent of the research team's access to an actual *da Vinci* Surgical System.

General Procedure

The design team will develop a solution using an iterative approach. The problem will first be identified as the design team communicates and exchanges ideas with both users of the device and clients. Once design objectives and constraints are identified, design alternatives will be proposed that meet the required system functionality previously specified in the problem statement. Conceptual alternatives will be evaluated against matrices and each design's feasibility of implementation will be evaluated. A final design of the device will be selected and constructed. The device's functionality will be verified. Future considerations and recommendations will be communicated.

This document is divided into chapters detailing the design team's work. The next chapter, the *literature review*, is intended to inform the reader of what is currently known about the problem the team is attempting to solve as well as construct a logical foundation for the approach the design team took in surmounting the challenge. Subsequently, the *project strategy* will present specifically the problem the team is attempting to solve and describe the challenge in terms of objectives and constraints. The *alternative designs* section will detail the necessary functions of the device and possible means. These lead to the development of our conceptual design alternatives, feasibility studies, implemented alternative designs, and experiments. The *design verification* chapter includes our methodology in developing our final design and the results of each component of our final design. In the *discussion*, the design team reflects on the resulting design in the context of existing research within the field. We determine the validity of assumptions made throughout the design processes, the limitations of our designs, and convince the reader that the design did indeed meet the objectives and constraints laid out before. The *final design validation* chapter provides a more detailed look at the final design and is written for an audience looking to continue the project work.

2. LITERATURE REVIEW

Telesurgery

Recently, there have been significant advances in telesurgery research. As Haidegger et al. (Haidegger, Benyo and Kovacs) mentions, the *da Vinci* surgical system is the most successful master-slave surgical system to date. Currently, the master system relays control signals to the slave system based on user input. The user decides where to position the robot based on visual feedback. Haidegger et al. suggest haptic feedback in addition to visual feedback could be very advantageous during the manipulation of telesurgical systems.

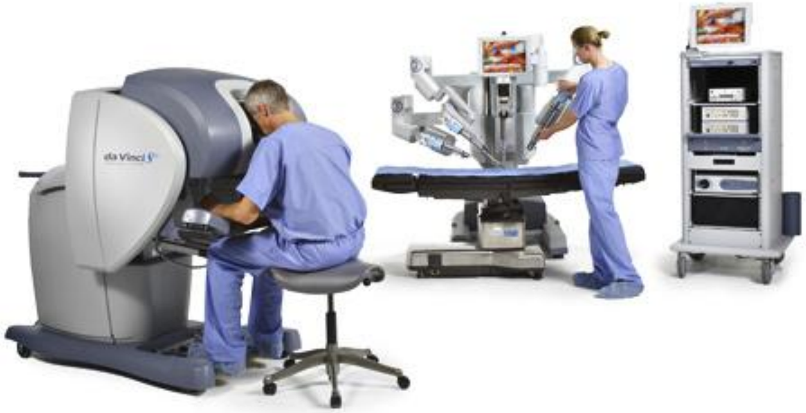

Figure 2.1: *Da Vinci* Teleoperated Surgical System. Pictured at the left is the master controller manipulated by the operator, to the right is the slave robotic manipulator **(Intuitive Surgical)**.

Berkelman and Ma (Berkelman and Ma) demonstrated that the physical footprint, weight and complexity of surgical robots can be drastically reduced while still allowing the robot to be just as, if not more, advantageous than their more cumbersome counterparts. These authors devised a robotic system which manipulates customized laparoscopic instruments allowing the robotic system to maintain the benefits of laparoscopic procedures such as being minimally invasive, reducing patient recovery time, and enhancing operator dexterity and visualization. However, their system is advantageous because it can be teleoperated by a surgeon some distance away and is small and lightweight enough to be mounted on a surgical table. Additionally, as the authors conclude, the small size of the robot enables lower actuating torque than traditional more massive surgical robots making this teleoperated robot inherently safer. Figure 2.2 illustrates the surgical robot Berkelman and Ma developed. Figure 2.3 depicts the increased precision associated with the researcher's teleoperated system over conventional laparoscopic manipulation.

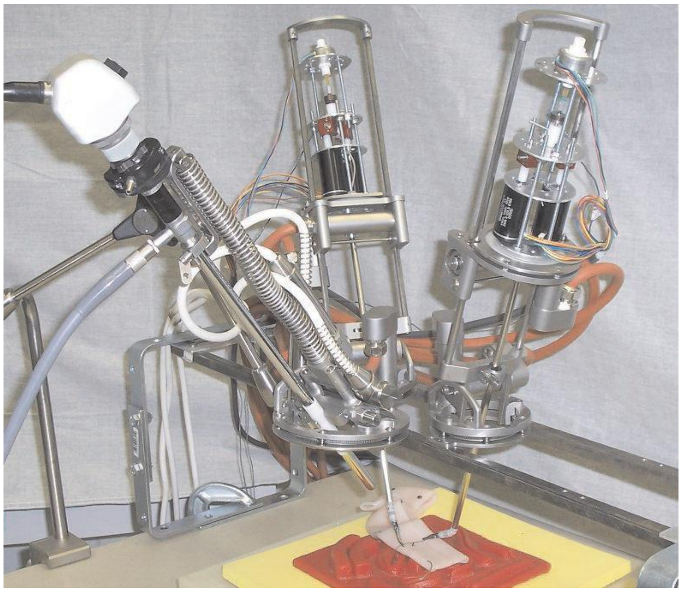

Figure 2.2: Portable teleoperated surgical robot (Berkelman and Ma).

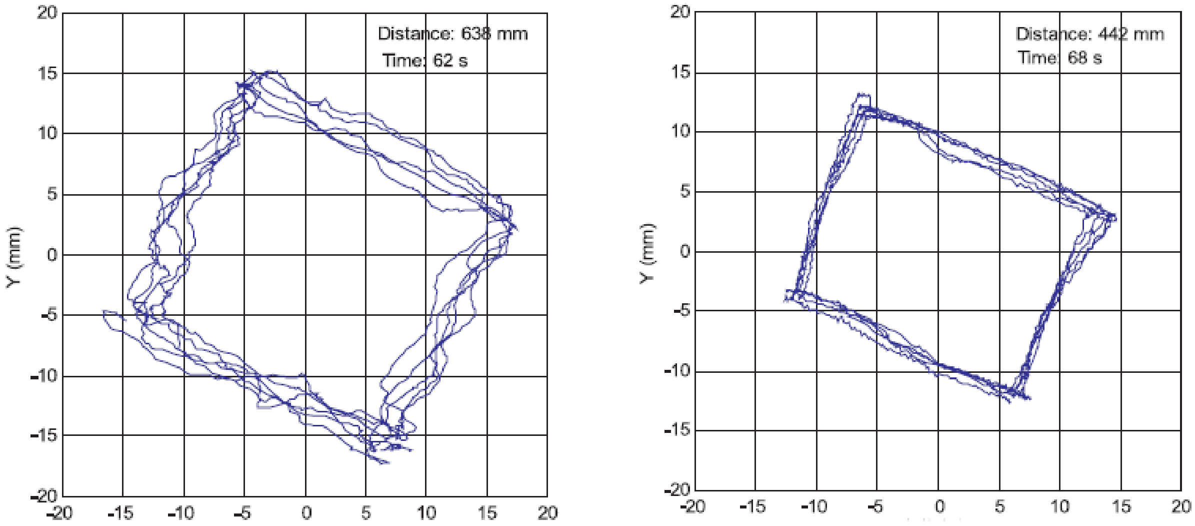

Figure 2.3: Berkelman and Ma demonstrated that their robot offers increased precision when compare to conventional laparoscopic manipulation (Berkelman and Ma).

Researchers at the University of Washington (Lum, Friedman and Sankaranarayanan) have demonstrated significant advancements in teleoperated robot research. Lum et al. developed the RAVEN, which is a master-slave telesurgical system. The robot utilizes two spherical manipulators which easily manipulate surgical instruments about a remote center. However, perhaps the most intriguing component of this research is the robot's teleoperation capabilities. For instance, the RAVEN (slave component of the surgical system) was deployed in Simi Valley, CA while the master surgeon console remained in Seattle, WA. Experiments were conducted and it was found that surgical maneuvers could be successfully accomplished given the communication latency. This mobile experiment yielded communication latencies of roughly 16 ms. These researchers also performed experiments with the RAVEN located in London, England and observed communication latencies averaging 75 ms. Figure 2.4 depicts the trajectory error due to communication latency observed by the researchers. It is also notable that an RTAI control system was used in developing the RAVEN.

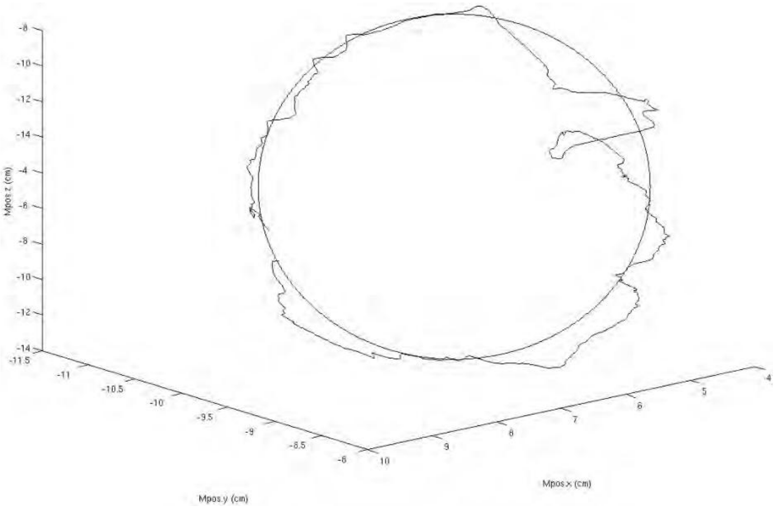

Figure 2.4: Trajectory error while RAVEN was stationed in London, England and master controller was stationed in Washington (Lum, Friedman and Sankaranarayanan).

Haptics and Force Sensing

Many researchers acknowledge the potential benefits of force feedback for robotic surgical tools. For instance, Ishii et al. recently developed a novel robotic forceps bending-manipulator (Ishii, Kobayashi and Kamei). The researchers envision their device easily relaying force feedback information to the operator during surgery. The desired ability for robotically manipulated surgical utensils to provide force feedback is an increasing trend.

Okamura (Okamura) explains that most commercially available telerobotic systems do not incorporate haptic feedback. The author provides motivation for haptics research including the ability for haptic feedback to enhance surgical simulation and better train practitioners. Additionally, with haptic feedback it may be possible to emulate tissue and potentially operate on a virtually still biological system.

Okamura conducted a very practical experiment to demonstrate how easy it is for cardiac surgeons to break fine sutures during robot-assisted surgery with no force feedback. Suture tensions were measured during knot tying. It was shown that suture tension was much higher when a robotic instrument was used to tie the suture compared to when the suture was tied by hand. Clearly force feedback would be a very practical and logical progression in robot-assisted surgery. Figure 2.5 illustrates Okamura’s experimental results.

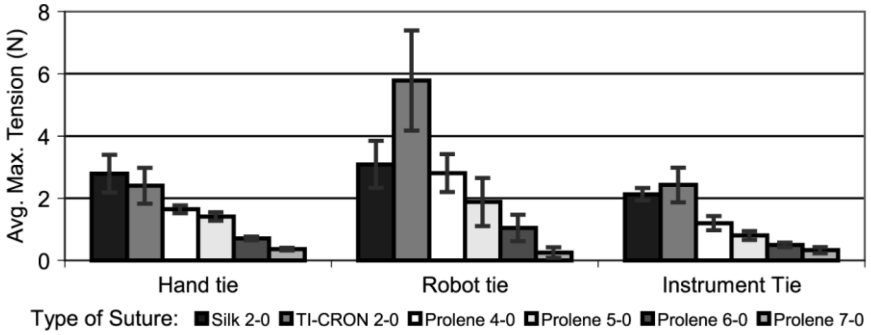

Figure 2.5: Suture tensions during hand and robot suture ties **(Okamura)**.

Research into the proper use and benefits of haptic feedback is necessary for the successful implementation of haptic feedback devices. Researchers at Johns Hopkins (Verner and Okamura) investigate the influence of additional haptic feedback degrees of freedom and whether or not they are necessary. The researchers explain how little research exists on whether complex feedback tasks incorporating both torques and Cartesian forces can be simplified into mere force feedback tasks. If properly understood, simplifications in feedback systems may lower costs, complexity, and the time it takes to successfully implement a force feedback system. Researchers found that during simple tasks force feedback can indeed be simplified and not impair usefulness. Specifically, force and torque feedback can be simplified into solely force feedback without observing significant performance differences in the simple task of drawing a circle.

Mahvash and Okamura (Mahvash and Okamura) have also conducted considerable research in minimizing the unwanted effects of the mechanical telesurgical system (friction and inertia) on force feedback. This optimization increases the clarity of force transmission between the slave to master components of system.

Da Vinci Research

Several groups have attempted to recreate the *da Vinci's* functionality. For instance, Sun et al. (Sun, Van Meer and Schmid) developed a software simulation of the *da Vinci* system for the purpose of surgical training. Their simulation modeled the surgical robot's 13 degrees-of-freedom. The simulation is controlled by two SensAble Phantom Omni devices fitted with custom finger grippers. The intent of the research is to facilitate *da Vinci* training, allowing an operator to experience a virtual system with identical functionality to the *da Vinci*. They envision their system reducing the *da Vinci* learning curve and being used to optimize trocar placement for surgical planning.

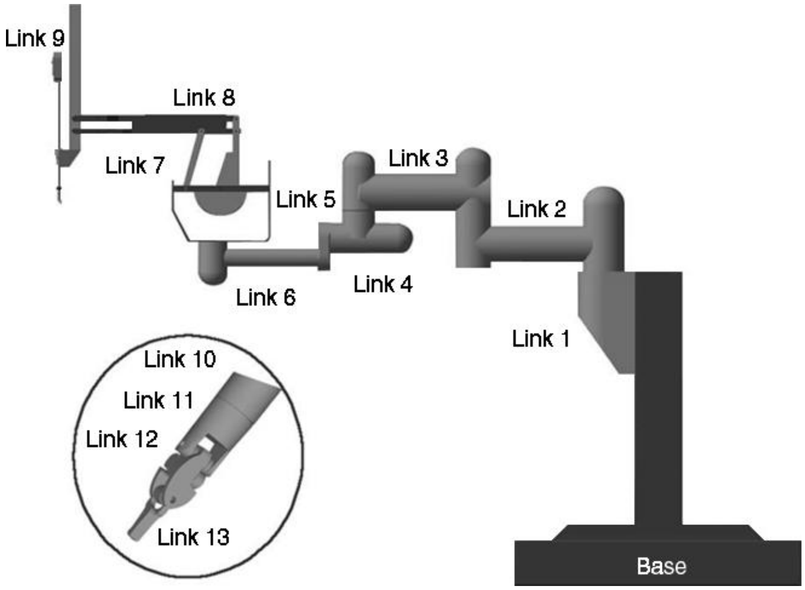

Figure 2.6: Robot definition for the virtual simulation of the *da Vinci* used by Sun et al. **(Sun, Van Meer and Schmid)**

3. PROJECT APPROACH

Initial Client Statement:

"Design a device to measure tool-tissue interaction forces during robot-assisted surgery and effectively relay these forces to the operator. Furthermore, develop a custom platform to articulate a da Vinci tool, emulating the functionality of the surgical robot."

As the reader can see, this initial client statement was not specific enough to yield an appropriate design. Further communication with our advisor and users of the device was necessary. The design team had the opportunity to discuss the idea of a force sensing module and custom platform for haptics research with Dr. Hiep T. Nguyen, the Director of Robotic Surgery Research and Training at Children's Hospital Boston.

Objectives and Constraints:

After several communications with our project advisor and a review of current research on the *da Vinci*, telesurgery, haptic feedback, and medical robotics in general, the team assembled the following list of objectives and constrains to describe our design challenge.

List 1. Haptic Device, Indented Objectives List

1. Compatible with existing instrument.
2. Easy to Use
    - 2.1 Minimal change in surgical technique
    - 2.2 Intuitive to operate
    - 2.3 Software interface is simple
    - 2.4 Easy to set up and connect.
3. Safe
    - 3.1 For user
    - 3.2 For the patient
4. Reliable
    - 4.1 Repeatable & Accurate representation of forces.
    - 4.2 Repeatable & Accurate control of end effecter
    - 4.3 Sturdy and able to withstand continuous use
5. Maintainable
    - 5.1 replace broken components

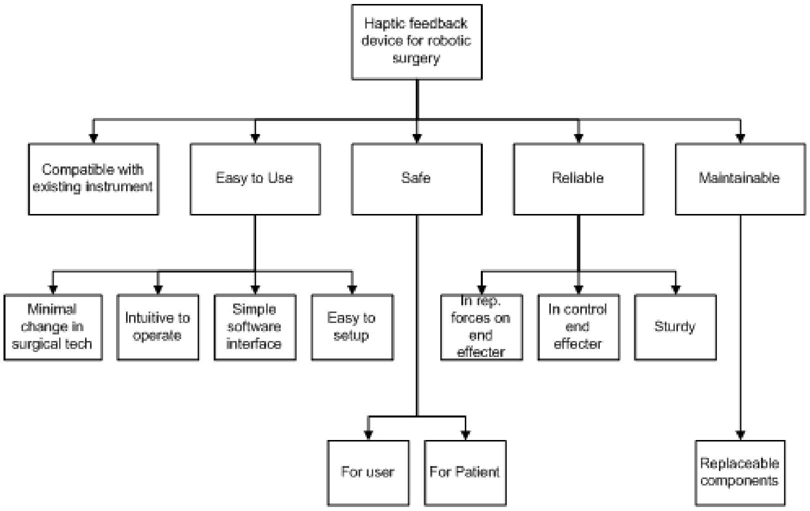
Haptic feedback device for robotic surgery
Compatible with existing instrument
Easy to Use
Safe
Reliable
Maintainable
Minimal change in surgical tech
Intuitive to operate
Simple software interface
Easy to setup
In rep. forces on end effecter
In control end effecter
Sturdy
For user
For Patient
Replaceable components

Figure 3.1: General objectives list and objectives tree for the sensing module and haptic feedback device.

Once these objectives were initialized, the design team sought a way to elicit from our advisor the most important objectives. Although all seemed important, the objectives needed to be prioritized. Accordingly, a pairwise comparison chart was used to weight the objectives and determine the priority of objectives relative to each other.

Table 3.1: Pairwise comparison chart used to prioritize objectives for the sensing module and haptic feedback device. It was determined that ease of use and compatibility were the primary objectives.

General Goals	Compatibility	Easy to Use	Safe	Reliable	Maintainable	Score
Compatibility	•••	0.5	0.5	1	1	3
Easy to Use	0.5	•••	1	1	1	3.5
Safe	0.5	0	•••	1	1	2.5
Reliable	0	0	0	•••	0.5	0.5
Maintainable	0	0	0	0.5	•••	0.5

The same process was repeated for the robotic research platform. Initially we brainstormed a list of objectives and subsequently attempted to narrow and prioritize the objectives through the use of pairwise comparison charts.

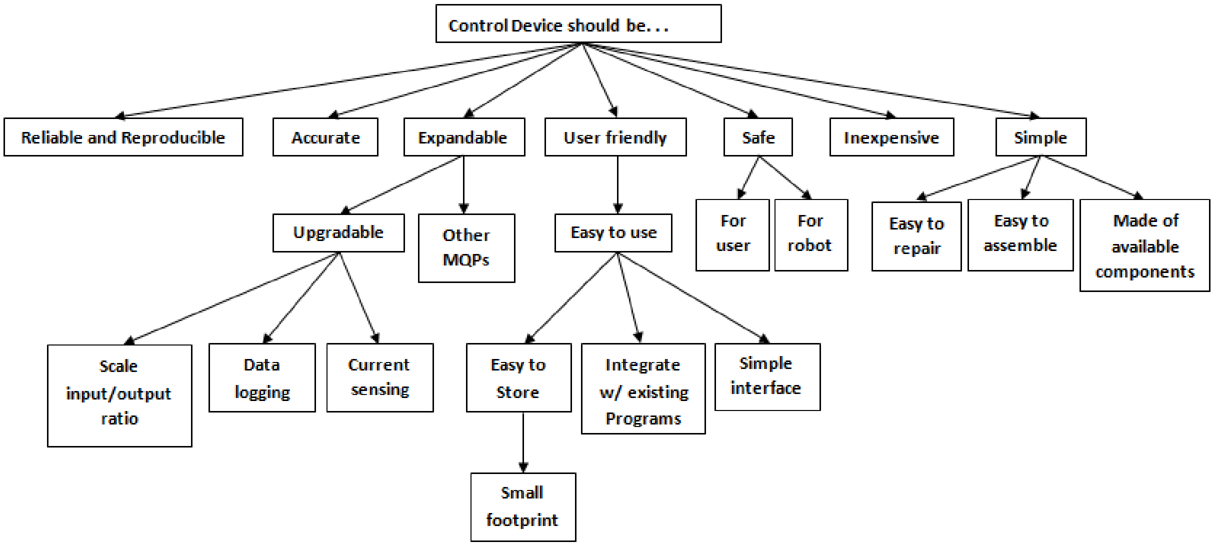

Figure 3.2: General objectives tree for the robotic research platform

Again, after a thorough list of objectives was created, we sought feedback from our advisor and by referring to literature in order to prioritize the objectives.

Table 3.2: Pairwise comparison chart used to prioritize objectives relative to one another for the robotic research platform

General Goals	Reproducible and Accurate	Expandable	User Friendly	inexpensive	simple	Score
Reproducible and Accurate	●●●	1	0	1	0.5	2.5
Expandable	0	●●●	0	1	1	2
User Friendly	1	1	●●●	1	1	4
inexpensive	0	0	0	●●●	0	0
simple	0.5	0	0	1	●●●	1.5

Overall, the high priority objectives for the project can be resolved into a concise list. This list was what the design team used to plan our conceptual designs in the next section.

List 3.1: Primary design objectives for the two primary subcomponents.

1. The force sensing module and haptic feedback device:

- ***Reliable sensing:*** The sensor module should reliably and accurately measure forces applied to the end effecter of the *da Vinci* surgical tool.
- ***Effective:*** Sensor data must be mapped to end effecter forces and this kinesthetic haptic feedback should be effectively represented to the operator.
- ***Compatibility:*** The sensor module should attach between the surgical tool and standard *da Vinci* positioning arm.

2. The robotic research platform:

- ***User Friendly Control:*** A dynamic Cartesian position and static remote center should be easily input by the user.
- ***Reproducible positioning:*** The platform should allow the surgical tool to be reproducibly positioned in real-time.

Next, the design needed to be realistically constrained from a variety of areas including spatial, financial, time, safety, and resources. A concise list of constraints was developed for each of the two major subcomponents before moving forward in the design process.

List 3.2: Design constraints for the two primary subcomponents.

1. The force sensing module and haptic feedback device must. . .

Constraint: Must not fall apart during simulated surgery

Constraint: Must not inhibit surgical procedure

Constraint: Prototype must not cost more than $300

Constraint: Must interface with standard *da Vinci* surgical tool and *da Vinci* arm

Constraint: Must be constructed from resources available through WPI

2. The robotic research platform must. . .

Constraint: Must fit on laboratory work bench

Constraint: Must build open existing industrial pick-and-place robot

Constraint: Prototype must not cost more than $300

Constraint: Must be safe and have emergency stop

Constraint: Must be constructed from resources available through WPI

Moreover, the design team spent considerable time determining what the device must actually do, or its functions. This step consisted of treating each subcomponent of the design as a figurative black box. Given a set of inputs and desired outputs, what must the device do to achieve appropriate mapping of inputs to outputs.

List 3.3: Functional requirements of the two major subcomponents

1. The force sensing module and haptic feedback will. . .

Function: Measure applied forces to end effecter of *da Vinci* surgical tool

Function: Measure position of end effecter

Function: Transmit force and positional data to the controller

Function: Actuate *da Vinci* tool based on positional information

Function: Transmit force data to the operator

2. The robotic research platform will. . .

Function: Articulate the *da Vinci* surgical tool with approximately the same degrees-of-freedom as Intuitive's *da Vinci* Surgical System.

a. Sense positional data from axes of the robotic platform

b. Generate and amplify command signals to actual robotic platform

Function: Interpret desired command position from user's physical input and scale

Function: Hold an arbitrary point along the tool shaft still to simulate tool-skin interface (remote center of motion).

Function: Allow the user to calibrate and zero the platform.

With the design space more thoroughly explored and subsequently constrained, it was possible for the design team to revise our client statement. Our objective with the revised client statement was to articulate exactly what was expected from the design while keeping the description as concise as possible.

Revised Client Statement:

"*Design a modular device to reliably measure tool-tissue interaction forces during robot-assisted surgery and effectively relay these forces to the operator. The device should be constructed for under $300 and integrate with the da Vinci Surgical System (preferably between the surgical tool and arm as to not inhibit the surgical procedure). Furthermore, develop a custom platform to articulate a da Vinci tool with the degrees-of-freedom of an actual da Vinci robot, while maintaining a remote center of motion. The platform should reliably control the position of the tool and easily translate the user's physical input into tool motion."*

4. ALTERNATIVE DESIGNS

Functional Specifications

Before the design team could conceptualize design alternatives, it was important to add specific values in order to quantify the listed device functionality. The most critical objective of this step in the design process was to identify the range of operation components should operate within. These specifications may be wrong, however since the design is methodical, they can easily be changed and the process repeated yielding a slightly modified design.

List 4.1: Design specifications associated with design functionalities

1. The force sensing module and haptic feedback device

Spec: Measure applied forces to end effecter of *da Vinci* surgical tool which range from approximately 0.25 to 6 Newtons during typical suturing maneuvers (Okamura). The design team then calculated corresponding maximum joint torques at the tool interface (T_{Joint}) to be roughly 0.2 Nm.

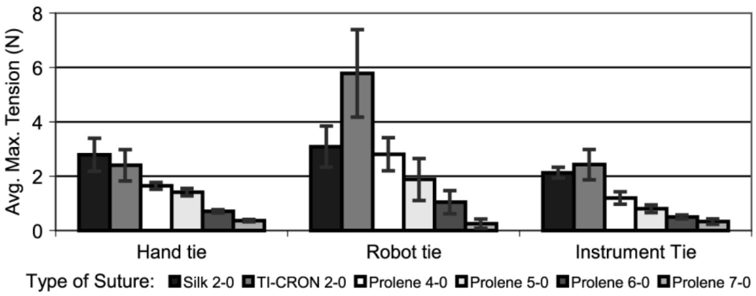

Figure 4.1: Average maximum tension during suture ties **(Okamura)**.

$$T_{Joint} = \frac{F_{Tip} L_{Tip} R_2}{R_1} = 0.18\ Nm$$

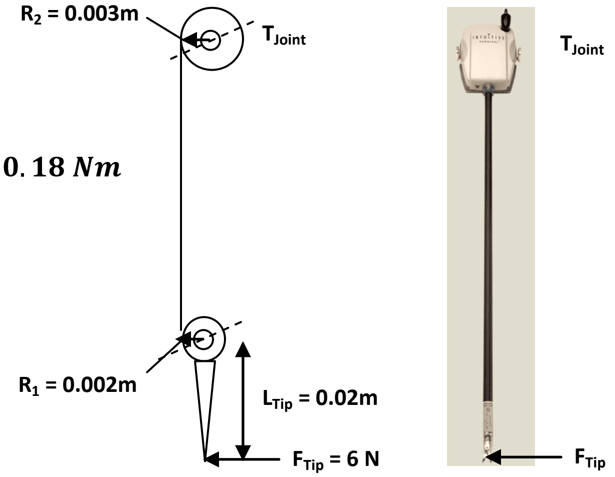

Figure 4.2: Corresponding surgical tool joint torque resulting from average maximum suture forces.

Spec: Measure position of end effecter via joint rotations with an error of at maximum ±0.7 degrees. This is the resolution a 500 count per revolution encoder will measure rotational motion in a joint.

Spec: Transmit force and positional data to the controller at a rate between 0.5 and 1.0 Khz. This is the industry standard for control loop execution.

2. The robotic research platform

Spec: Articulate the *da Vinci* surgical tool with 6 degrees-of-freedom, 3 positional and 3 orientation (Sun, Van Meer and Schmid).

a. Sense positional data from axes of the robotic platform with an error of at maximum ±0.7 degrees. This is the resolution a 500 count per revolution encoder will measure rotational motion in a joint.

b. Generate and amplify command signals to actual robotic platform. 6 signals (one for each necessary joint actuator) should saturate at -12 and +12 volts (bi-directional control) and supply 2 amps continuous and 3 to 4 amps peak. (to overcome frictional and inertial torques at each joint while linearly accelerating to a peak velocity of 0.6 radians per second). This information was determined empirically from the industrial pick-and-place robot.

Spec: Hold an arbitrary point along the tool shaft still to simulate tool-skin interface (remote center of motion). Should appear visually still and remote center should move with a maximum error of ±5mm (tolerable skin stretch).

Research Platform

Conceptual Alternatives Generation

The design team started to generate conceptual design alternatives by using a morphological chart where functions are specified and various means for achieving each function are specified. Below is a morphological chart corresponding to the research platform component of the design challenge.

Table 4.1: Morphological chart (functions and possible means) for the robotic research platform.

Function	Means				
Interpret Encoders of industrial robot	5 microcontrollers & RS232	4 Diff. encoder ICs & 1 mater microcontroller & RS232	Neuron Robotics Board	Labview DAQ with diff. encoder support	
Interpret command position from user	Purchase joint stick & serial interface	Purchase Falcon & serial interface	Custom cradle linkage with potentiometers	Software control knobs and sliders	Hardware control knobs and sliders
Scale and map inputs	Software scaling	Hardware scaling			
Run control loop	On microcontroller	Labview VI, control toolbox	Matlab, simulink control tool box	Embedded Linux	SIST software in AIM lab
Generate command signal	DAC IC, serial	DAC PC104 card	Microcontroller, serial	Labview DAC	
Amplify command signal	Linear amplifiers LDH-S3	Switching amplifiers	Large op-amp	H-bridge	

LabView-based Control System

Based on this brainstorming, three promising alternatives arose for the platform. The first alternative is shown in Figure 4.3 and consisted of a LabView based control system, using a LabView specific data acquisition system (DAQ). The DAQ will read raw quadrature encoder inputs and additionally onboard DACs will be used to generate control signals. Inverse kinematics and computations will be done using LabView's graphical programming and a Virtual Instrument will be created. Linear amplifiers would be used to amplify the control signals and either a joystick or software knobs would register user input.

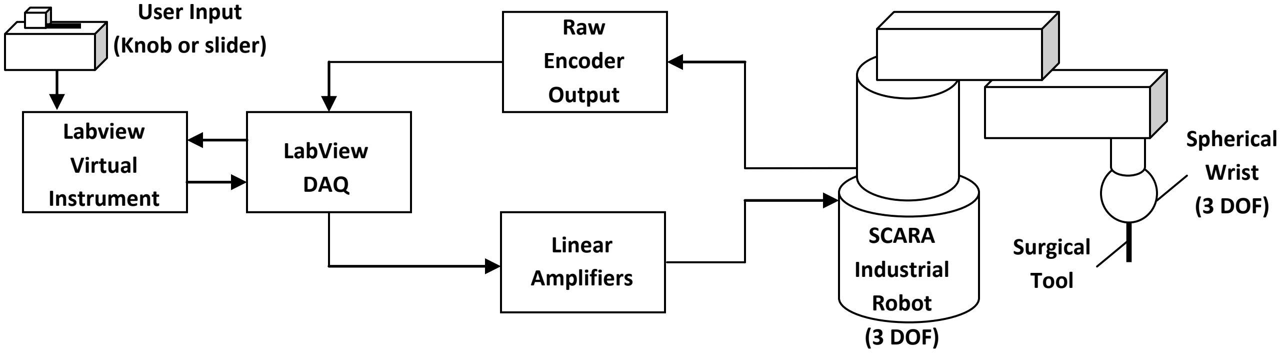

Figure 4.3: First conceptual alternative, LabView based robot control system.

Linux-based Control System

A second design alternative depicted in Figure 4.4 consisted of a Linux based control system. Here, raw encoder output would first be processed by purchased integrated circuits specifically intended to input quadrature signals and output a 16-bit count via serial communication. A low level microcontroller would be in charge of requesting positional data from each counter IC. The low level microcontroller would then communicate via serial to an embedded Linux computer, which would execute high level processing and generate control signals. A PC104 card with DACs would be used to output control signals to a series of linear amplifiers controlling the robot's DC motors.

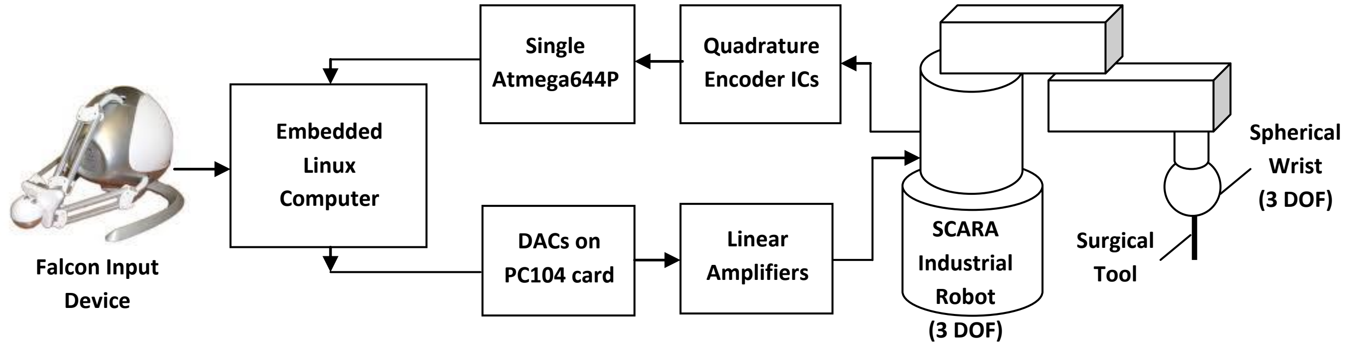

Figure 4.4: Second conceptual alternative, Linux hierarchical based robot control system.

Microcontroller Control System

The final alternative design illustrated in Figure 4.5 consisted of moving the entire control system to an embedded microcontroller. The alternative consists of using an 80Mhz PIC microcontroller. On board external interrupts will be utilized to count quadrature encoder pulses, and on board DACs will be utilized to output command signals. Internal clocks will be used to generate an interrupt driven control loop to compute joint positions from user input utilizing robot kinematics. As in the above alternatives, linear amplifiers are employed to amplify control signals. User input can take the form of hardware knobs and sliders or a possible falcon controller.

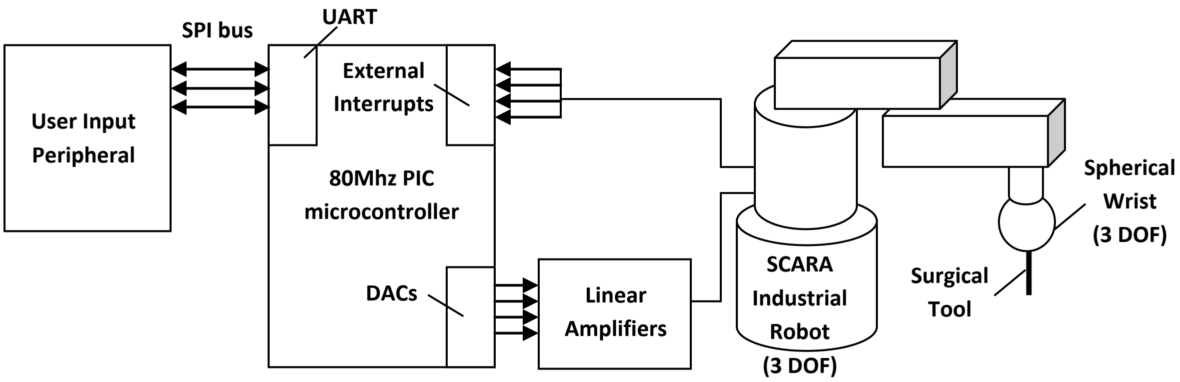

Figure 4.5: Third conceptual alternative, Microcontroller based robot control system.

Preliminary Data and Feasibility

The design team began to look at the alternative *da Vinci* research platforms critically and determine which alternative was indeed feasible and could meet the outlined design objectives. We began by evaluated the LabView based control system. A simple serial communication Virtual Instrument example was used to evaluate the real-time capabilities of LabView running in a Windows environment without specialized real-time hardware such as National Instrument's cRIO. The provided default serial communication instrument was slightly modified. From this initial experiment, the design team concluded that a reliable 1 ms control loop could not be established. The tested loop wrote a request character to a low level AVR microcontroller and subsequently read several bytes transmitted from the microcontroller, and finally cleared the serial buffer.

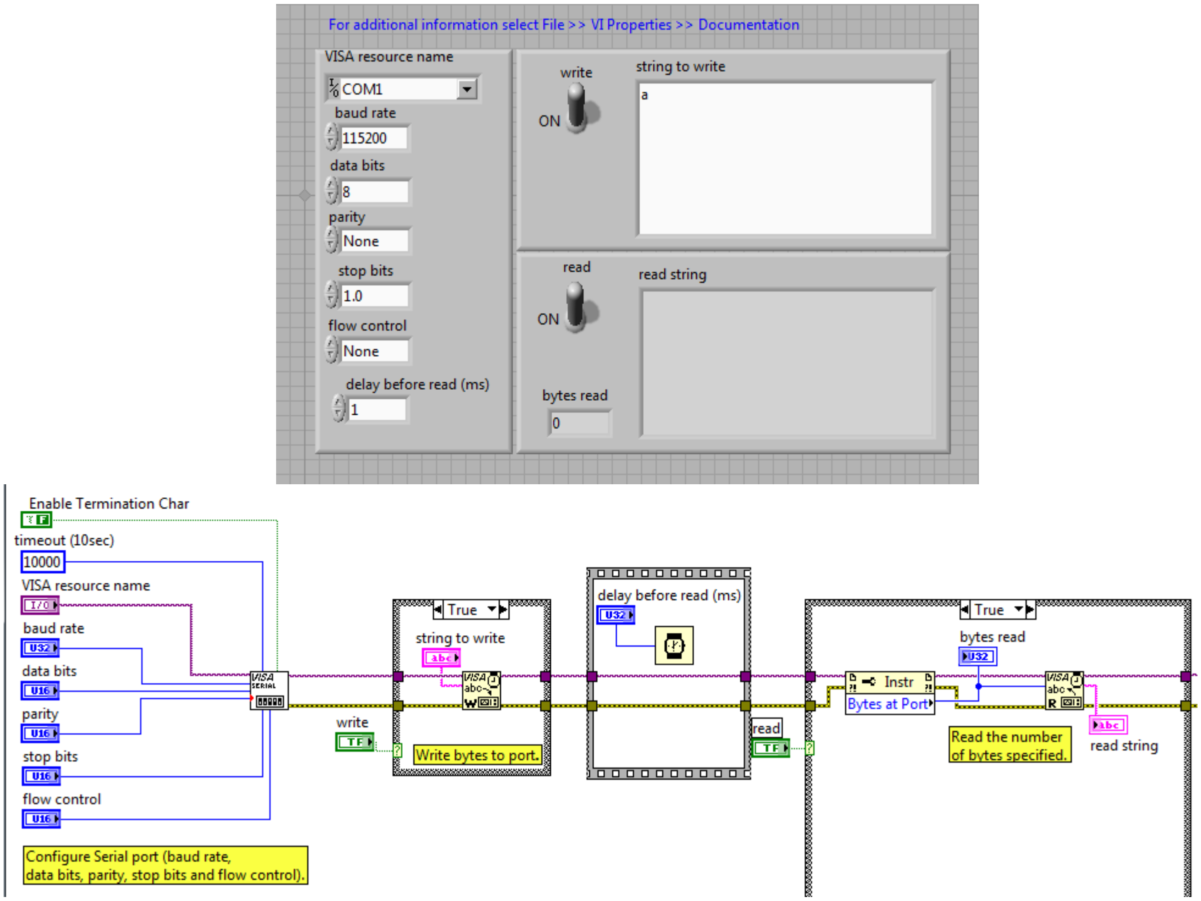

For additional information select File >> VI Properties >> Documentation

VISA resource name: COM1

baud rate: 115200

data bits: 8

parity: None

stop bits: 1.0

flow control: None

delay before read (ms): 1

write: ON

string to write: a

read: ON

bytes read: 0

read string

Figure 4.6: Virtual Instrument used during initial experiments with LabView system.

Given these results, the design team concluded that this alternative was not feasible. A clear design object was for the platform to reliably run a 0.5 to 1 Khz control loop.

Looking for a real-time solution, the design team next evaluated the possibility of moving the control system to a single microcontroller, design alternative three. Using the PIC microcontroller in conjunction with an external 80Mhz oscillator, a reliable 1Khz interrupt could easily be achieved. The inverse kinematics calculations required to determine the robot's joint angles and the collection of sensor input through both analog to digital converters and serial communication could, with conservative fixed point mathematics, be moved to the microcontroller. The major disadvantage to this alternative is the lack of processing downtime. In terms of usability and user interface, having a PC and monitor would be much more familiar and friendlier. For the reasons of simple user interfacing, the design team chose to reject this design alternative.

The Linux based control system, shown in Figure 4.4, was chosen for the robotics research platform. This alternative was the only alternative that met the functional specifications of being able to reliably produce a 0.5 to 1 Khz real-time control loop, allow easy interfacing with the user and more complicated peripheral devices as well as easily handle the magnitude of calculations, sensor reading, and serial communication necessary for the research platform.

To validate this alternative a vanilla Linux kernel (version 2.6.28.7) was patched with RTAI (version 3.6.1) and re-complied on Ubuntu 8.10. The real-time kernel provides a hardware abstraction layer (HAL) enabling reliable microsecond timing under a Linux operating system. Through considerable time and efforts, the installation of RTAI and the recompilation of the kernel were achieved (please see final design for a more detailed explanation). Ultimately, the design team was able to run a simple control process in real-time at 500 Hz. Timing was confirmed by modulating a digital IO pin during and observing the output on an oscilloscope. In the final system, the timing was set to 1kHz.

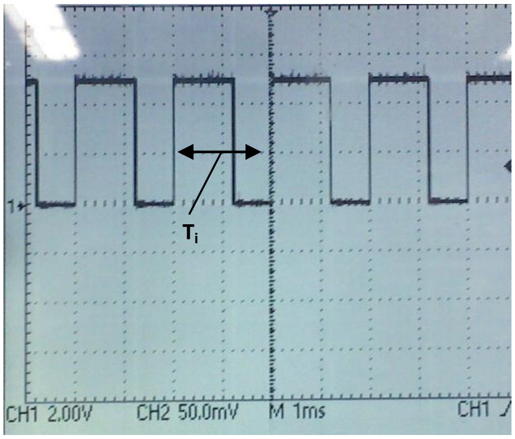

Figure 4.6: Validation of RTAI control process timing. Horizontal axis is set to 1 ms/dev. Period between control loop executions (T_i) is at a consistent 2ms.

Sensor Module

Conceptual Alternatives Generation

The design team brainstormed several effective ways to measure and relay forces and positional data as well as actuate the *da Vinci Surgical* tool. Again, the team resorted to constructing a morphological chart to organize potential conceptual alternatives. Here, a variety of means for achieving each of the subcomponent's primary functionalities were outlined.

Table 4.2: Morphological chart detailing means to achieve desired primary functions of the sensor module

Function	Means		
Measure kinesthetic bulk forces on end effecter	Force sensor (pad) applied to points of tissue contact	Measure tool joint torques with custom torque sensor	Measure tool joint torques with current sensing
Measure and actuate wrist of surgical tool	Closed loop: Encoders and small DC motors	Open loop: small stepper motor	
Transmit Haptic forces to user	Falcon Haptic Device	Custom cradle	Phantom Haptic Device

Force Sensing Pads

Several alternatives were formulated. The first of these alternatives was to utilize circular force sensing pads placed on critical tool-tissue interaction points. These sensors' signals will be amplified and relayed to the central processor. The surgical tool will be actuated by a set of DC motors with shaft encoders to measure position. Figure 4.7 shows a conceptual sketch of this alternative.

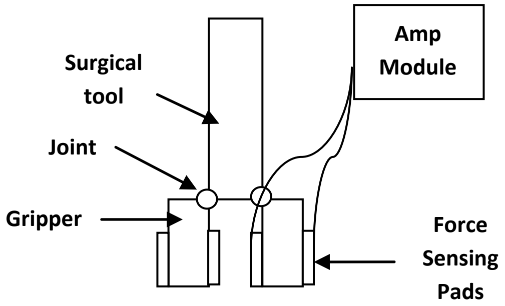

Figure 4.7: First design alternative for sensing module. Force pads placed on critically tool-tissue interaction locations monitor tool tip forces. An amplifier board is used to condition the signals.

Current Sensing

Secondly, the design team envisioned using a current sense resistor to measure applied motor torque on each of the four surgical tool joints. The alternative is illustrated in Figure 4.8 and is adapted from a concept found in a recent publication (Mahvash and Okamura). This alternative requires having a rough model of the DC motors used to actuate the tool in order to understand the relationship between current through the armature and applied motor torque (typically a constant, K_T). The motor, modeled as a resistor, inductor, and voltage source in series, has the same current ($I_{armature}$) passing through all its components. Another resistor, R_{sense}, is added in series. If the voltage differential over the current sense resistor is measured, via an instrumentation amplifier, and the resistance value is known, then the current in the series circuit is easily determined. Joint torques will be related to end-effecter Cartesian forces by empirically determining a Jacobian matrix describing the surgical tool. The method used to actuate and measure tool position is the same as in the previous alternative.

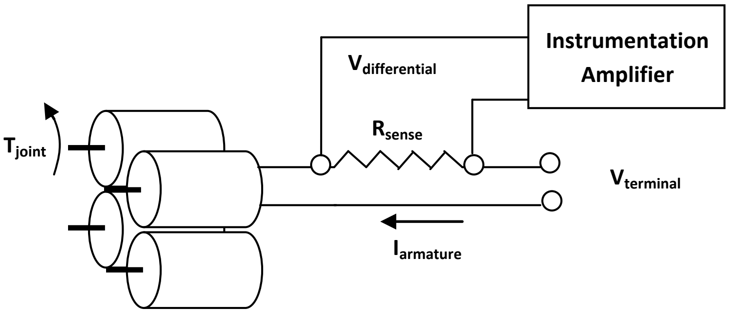

$$T_{Joint} = \frac{K_T V_{differential}}{R_{sense}}$$

Figure 4.8: Second design alternative for sensing module. Current through the armature is measured via a current sense resistor and this current is related to the torque output of the motor through a physical constant describing the motor's behavior.

Custom Torque Sensor

Thirdly, the design team developed an alternative based on custom torque sensors to measure joint torques directly. This alternative is illustrated in Figure 4.9. Each sensor is meant to act as a coupler between the actuating motor and *da Vinci* surgical tool control surface. The coupler will be engineered such that it intentionally elastically deforms under rotational torque. The deformation in the material will be measured by strain gages. The gages will be assembled in a full bridge arrangement such that under mechanical load the bridge will become unbalanced. An instrumentation amplifier will be used to capture this voltage differential. Below are conceptual designs the team created of couplers meant to deform elastically under applied torque.

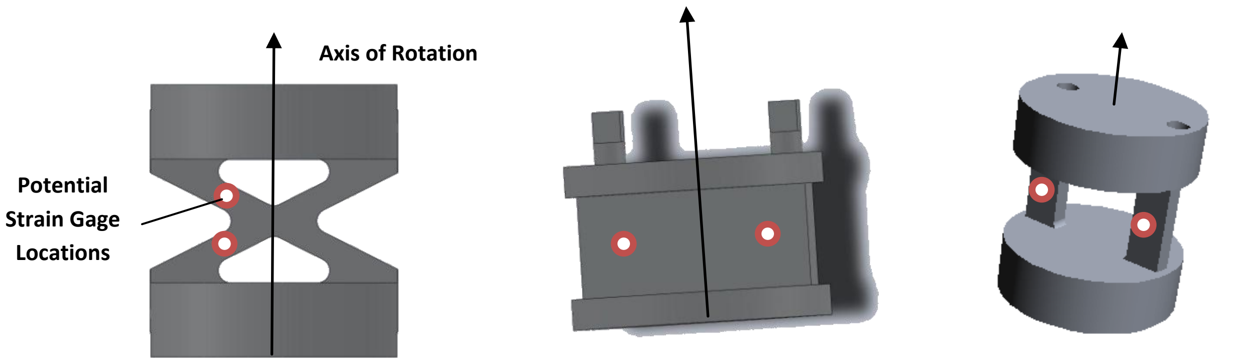

Figure 4.9: Third design alternative for sensing module consisting of deformable couplers to measure joint torques. Joint torques will subsequently be translated to the surgical tool's Cartesian tip force via a Jacobian.

Preliminary Data and Feasibility, Sensor Module

The team heavily considered the constraints and objectives of the project while evaluating the feasibility of alternatives. For example, the first alternative, placing force sensing pads at tool-tissue interaction points, requires considerable modification to the *da Vinci* surgical tool and a major objective of the project is for the device to easily integrate into and work with the existing surgical system. The fact that this alternative requires each tool to be individually modified is unacceptable from the perspective of compatibility.

Additionally, the current sensing alternative offered a very compact, reliable solution. This alternative does not seem to spatially interfere with the surgical procedure and requires minimal moving components adding to safety and reliability. However, the primary problem the design team saw in this alternative was that the *da Vinci* motors are not accessible to the user and the addition of a sensing resistor would require modification to the existing equipment. This directly contradicts the team’s design constraints making this alternative infeasible.

The best alternative that the design team conjured was a module containing four external joint torque sensors, as are depicted in Figure 4.9. The module is intended to integrate between the *da Vinci* surgical tool and the *da Vinci* arm faceplate. This design would not require any modification to the existing device. The seamless integration of this alternative offered with existing technology seemed to outweigh the challenge presented in creating its torque sensing elements. For these reasons, this alternative was chosen.

5. FINAL DESIGN METHODOLOGY

Overall System Architecture

The overall system contained mechanical, electrical, and software subsystems. Figure 5.1 illustrates the overall final design. The proper integration of these subsystems yielded the design's functional requirements outlined in the previous sections. The team developed the following major subcomponents:

- Custom Spherical Wrist
- Surgical Tool Actuator Module
- Sensing Elements, Signal Amplifiers, and Sensor Module
- Electronics for Control System
- Software for Control System
- Haptic User Interface

The design was centered on the use of a Sony SCARA industrial robot acquired previously by the research laboratory. The robot offered 4 independent degrees-of-freedom. In accordance with the team's design objectives, 2 additional degrees of freedom were necessary to specify the surgical tool's orientation and maintain a remote center of motion. To achieve this functionality, a custom 2 degree-of-freedom spherical wrist was designed and implemented. In order to measure tool-tissue interaction forces, a sensing module capable of measuring surgical tool joint torques was employed. This module's main feature is its capacity to mount seamlessly in-between the *da Vinci* surgical tool and arm, emulating both male and female *da Vinci* connections on the corresponding faces of the module. This module housed 4 sensing elements, intended to elastically deform under torque. Strain gages arranged in a full-bridge converted this mechanical disturbance into a potential difference. The voltage differential was amplified using 4 instrumentation amplifiers and sampled using 4 analog to digital converters present on the embedded single board PC. These torques were mapped to end-effecter tip forces in the control process and output to the haptic user interface.

The robot was actuated based on the user's desired position input. This was acquired at the haptic user interface. The 6 degree-of-freedom robot's inverse kinematics were utilized in the control process to determine corresponding joint angles from the user's desired Cartesian end-effecter position. PID controllers were used at each joint to control joint angles. As mentioned, the set values for the controllers came from the results of inverse kinematic calculations. The actual position was measured using rotary encoders at each joint. Quadrature counter integrated circuits were utilized to count quadrature signals coming from the encoders and a single Atmega microcontroller was used to request positional information from each of the 6 joints. Communicating through a serial port, the high level embedded Linux control process requests all positional information from the low level Atmega microcontroller.

Resulting control signals were output through digital to analog converts on a PC104 card. Subsequently, command signals were amplified using moderately high-current linear amplifiers and sent to the robot's 6 DC motors. Lastly, a module capable of actuating the surgical tool was necessary for the research platform. This component housed four additional DC motors and an actual *da Vinci* arm disposable face plate.

The control process and peripheral communication were written in C and C++ code in Linux User Space. Real-time synchronization was maintained via Linux Kernel Space modules and the implementation of a RTAI kernel patch.

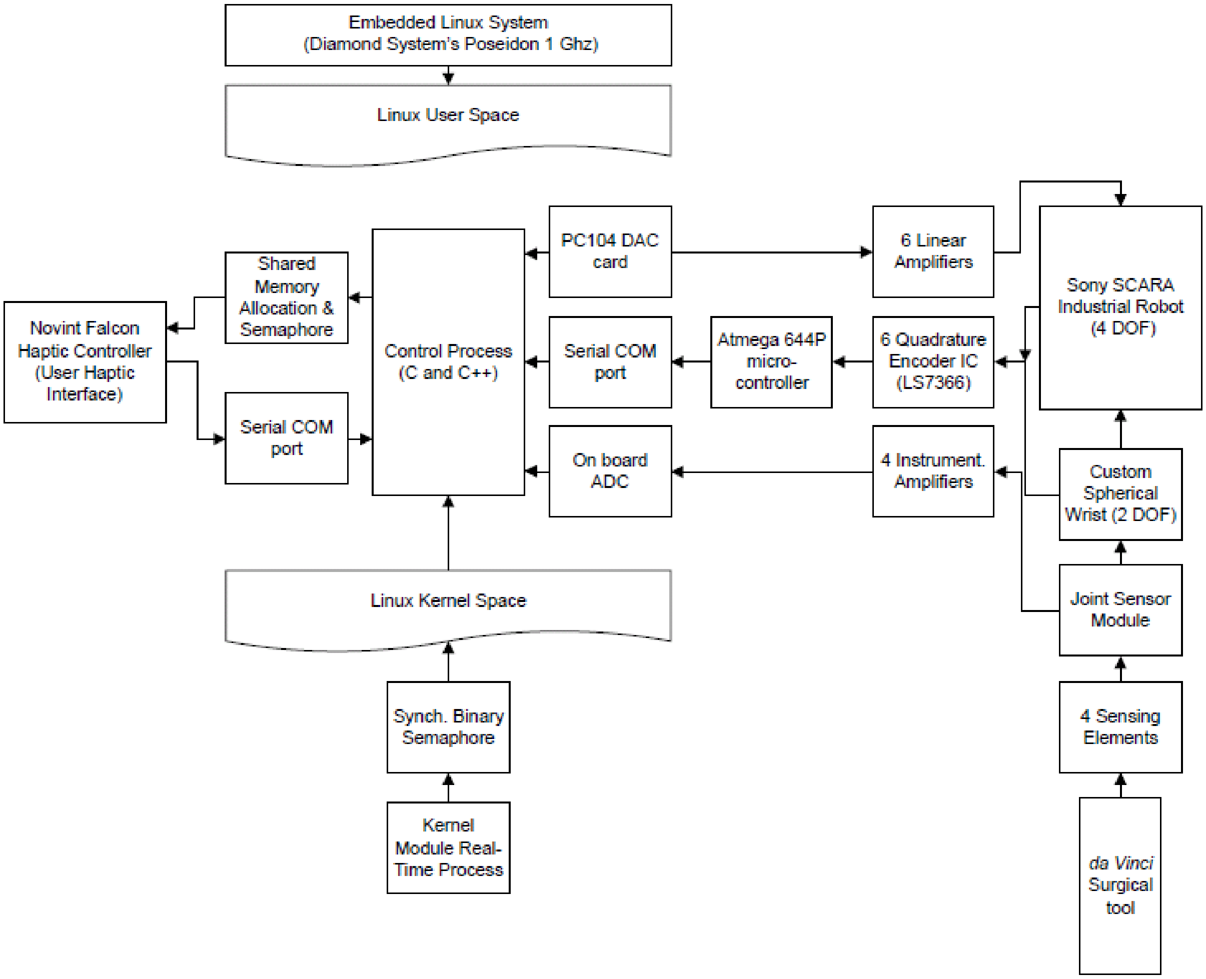
Embedded Linux System
(Diamond System's Poseidon 1 Ghz)
Linux User Space
Shared Memory Allocation & Semaphore
Control Process (C and C++)
PC104 DAC card
6 Linear Amplifiers
Sony SCARA Industrial Robot (4 DOF)
Novint Falcon Haptic Controller (User Haptic Interface)
Serial COM port
Atmega 644P micro-controller
6 Quadrature Encoder IC (LS7366)
Serial COM port
On board ADC
4 Instrument. Amplifiers
Custom Spherical Wrist (2 DOF)
Joint Sensor Module
Linux Kernel Space
Synch. Binary Semaphore
Kernel Module Real-Time Process
4 Sensing Elements
da Vinci Surgical tool

Figure 5.1: Overall flow of system architecture including major subcomponents

Sensing Element, Amplifiers, and Sensor Module.

Monitoring of tool-tissue interaction was achieved by measuring surgical tool joint torques. As shown in the preliminary calculations, tool tip interaction forces resulted in related joint torques.

Sensor Element

Sensing elements coupling to each joint were designed to intentionally elastically deform under torque and the resulting deformation was sensed using strain gages arranged in a full Wheatstone bridge. A mathematical model was first utilized to determine the physical parameters of the sensing element. Parameters were adjusted until a suitable voltage difference resulted and the physical dimensions were still feasible to manufacture. Assumptions included the two vertical members being modeled as a simple end-fixed cantilever beam. Applied joint torque was determined from design specifications and a safety factor of 4 was incorporated to emulate a worst case scenario of the DC motor outputting stall torque (0.6 Nm). Additionally, the strain measurement is averaged across the footprint of the gage, resulting in a very conservative strain estimate (200 με). Figure 5.2 depicts these calculations.

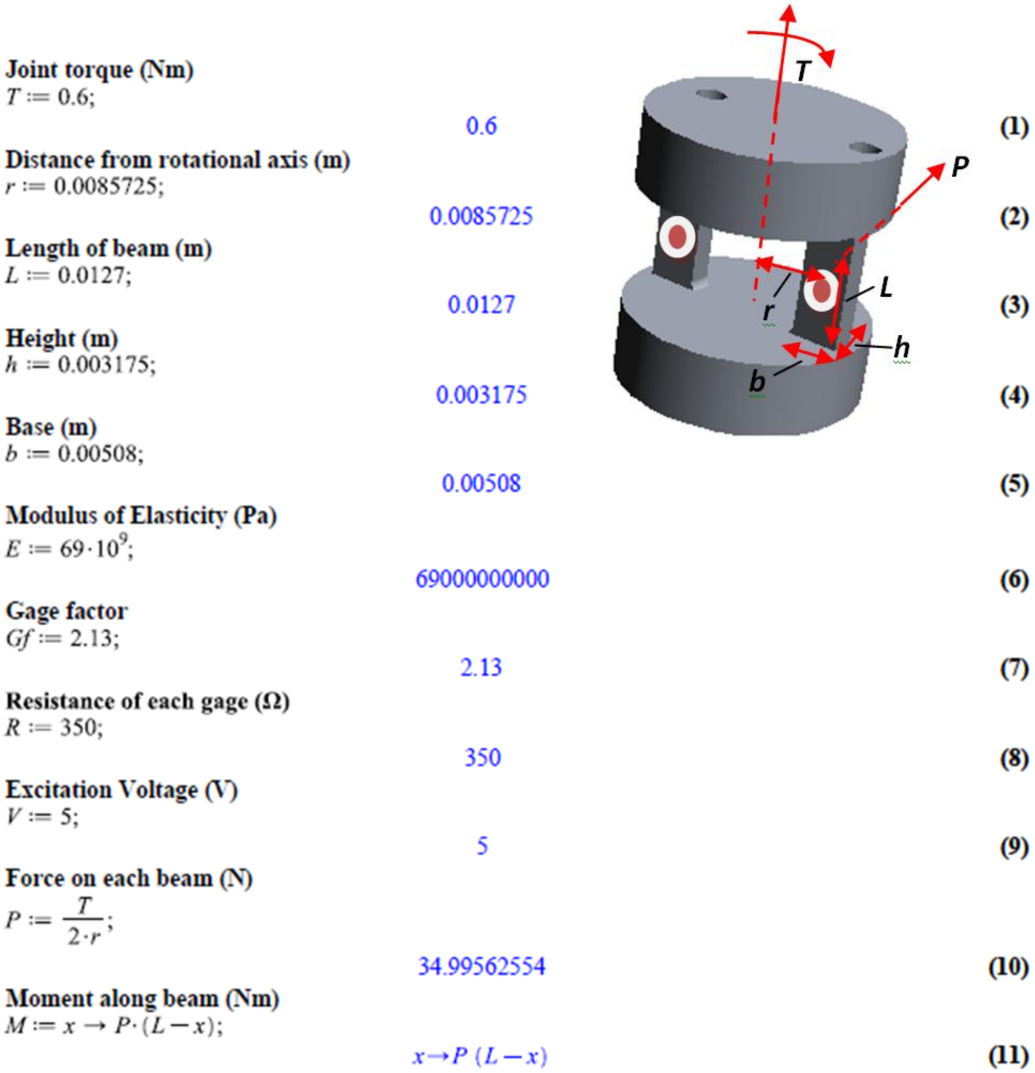

Joint torque (Nm)
$T := 0.6;$

$$0.6 \qquad (1)$$

Distance from rotational axis (m)
$r := 0.0085725;$

$$0.0085725 \qquad (2)$$

Length of beam (m)
$L := 0.0127;$

$$0.0127 \qquad (3)$$

Height (m)
$h := 0.003175;$

$$0.003175 \qquad (4)$$

Base (m)
$b := 0.00508;$

$$0.00508 \qquad (5)$$

Modulus of Elasticity (Pa)
$E := 69 \cdot 10^{9};$

$$69000000000 \qquad (6)$$

Gage factor
$Gf := 2.13;$

$$2.13 \qquad (7)$$

Resistance of each gage (Ω)
$R := 350;$

$$350 \qquad (8)$$

Excitation Voltage (V)
$V := 5;$

$$5 \qquad (9)$$

Force on each beam (N)
$P := \frac{T}{2 \cdot r};$

$$34.99562554 \qquad (10)$$

Moment along beam (Nm)
$M := x \rightarrow P \cdot (L - x);$

$$x \rightarrow P\ (L - x) \qquad (11)$$

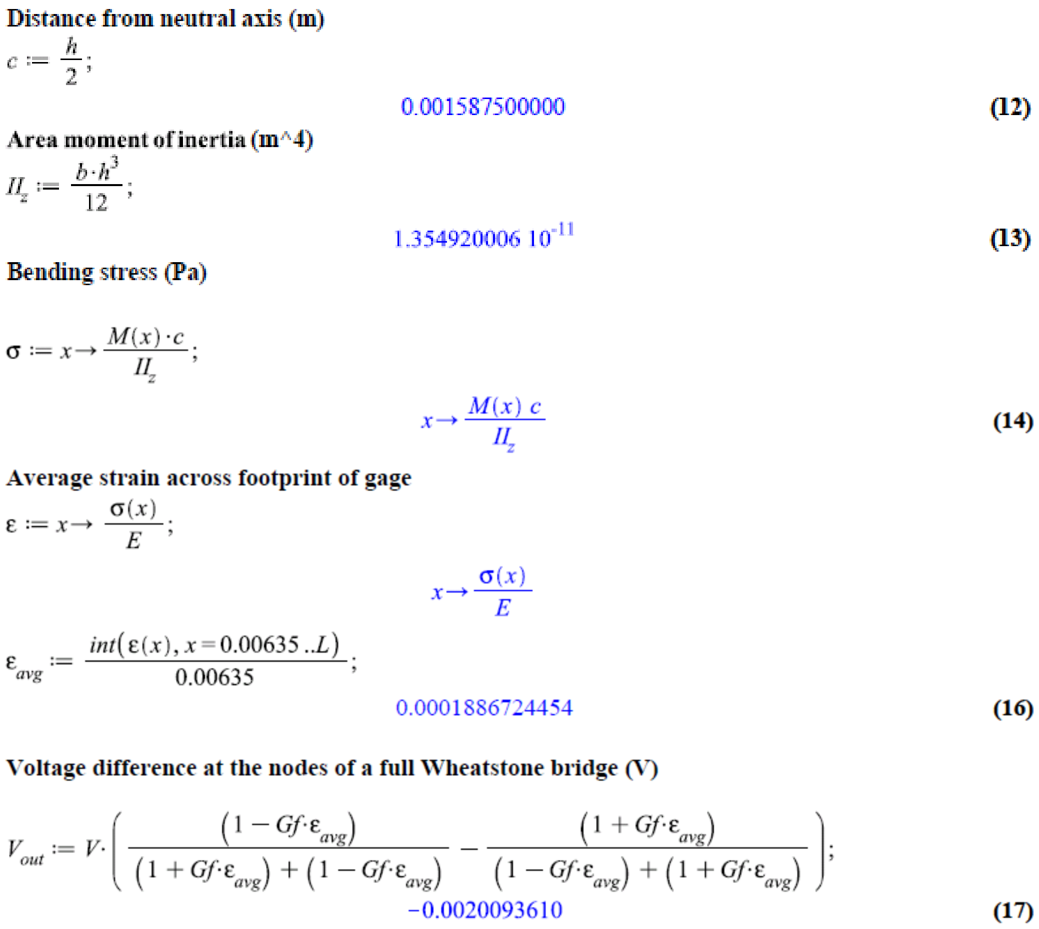

Distance from neutral axis (m)

$$c := \frac{h}{2};$$

$$0.001587500000 \qquad \textbf{(12)}$$

Area moment of inertia (m^4)

$$II_z := \frac{b \cdot h^3}{12};$$

$$1.354920006\ 10^{-11} \qquad \textbf{(13)}$$

Bending stress (Pa)

$$\sigma := x \rightarrow \frac{M(x) \cdot c}{II_z};$$

$$x \rightarrow \frac{M(x)\ c}{II_z} \qquad \textbf{(14)}$$

Average strain across footprint of gage

$$\varepsilon := x \rightarrow \frac{\sigma(x)}{E};$$

$$x \rightarrow \frac{\sigma(x)}{E}$$

$$\varepsilon_{avg} := \frac{int(\varepsilon(x), x = 0.00635\ ..L)}{0.00635};$$

$$0.0001886724454 \qquad \textbf{(16)}$$

Voltage difference at the nodes of a full Wheatstone bridge (V)

$$V_{out} := V \cdot \left(\frac{\left(1 - Gf \cdot \varepsilon_{avg}\right)}{\left(1 + Gf \cdot \varepsilon_{avg}\right) + \left(1 - Gf \cdot \varepsilon_{avg}\right)} - \frac{\left(1 + Gf \cdot \varepsilon_{avg}\right)}{\left(1 - Gf \cdot \varepsilon_{avg}\right) + \left(1 + Gf \cdot \varepsilon_{avg}\right)} \right);$$

$$-0.0020093610 \qquad \textbf{(17)}$$

Figure 5.2: Mathematic model used to determine physical dimensions of sensing elements and resulting magnitude of voltage potential.

Subsequently, the team used finite element modeling in SolidWorks (SolidWorks Corp., Concord, MA, USA) to confirm the mathematical model and optimize the placement of strain gages on the bending cantilever-like beams of the sensor element. Figure 5.3 details the finite element modeling.

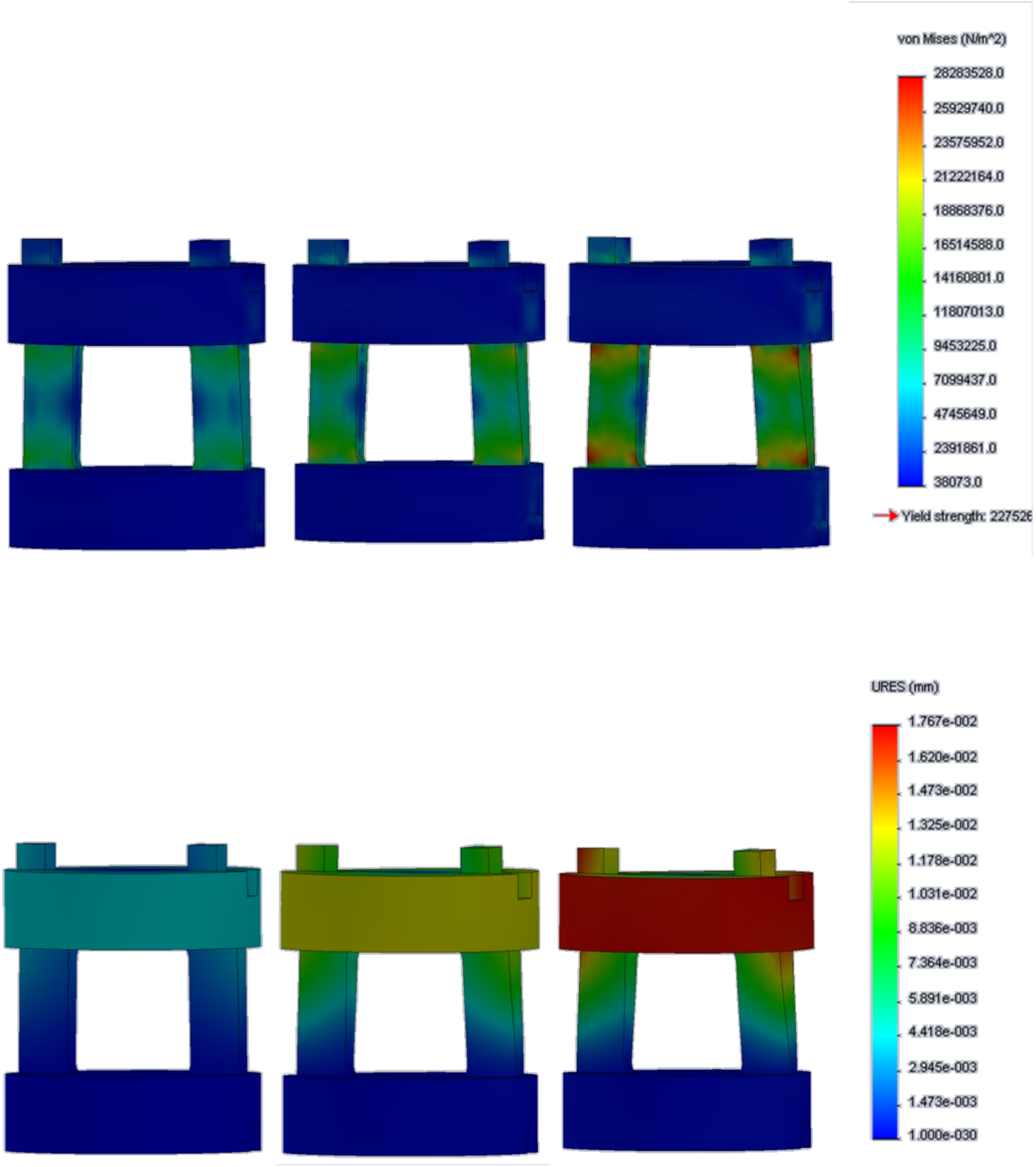

Figure 5.3: Gradual propagation of stress and strain resulting from applied torque (0.6 Nm) about the axis of rotation. The max deflection at max torque was < 0.02mm.

The actual sensor elements were machined from 1 inch precision ground 6061 aluminum on a manual Bridgeport machine. All critical dimensions were confirmed to have tolerances within ±0.005

inches. Each sensing element was populated with 4 Vishay CEA-13-125UN-350 strain gages (Vishay Intertechnology, Inc., Malvern, PA, USA). These gages are designed to be most sensitive in the range 1000 με. The design team determined our strain (200 με) to be on this order of magnitude. Additionally, 4 gages in a full Wheatstone bridge arrangement enable 4 times the measurement sensitivity. It was decided to keep the sensing elements as stiff as possible to increase ease of manufacturing and make feasible a wider variety of machining operations. Figure 5.4 details the actual assembled sensing element.

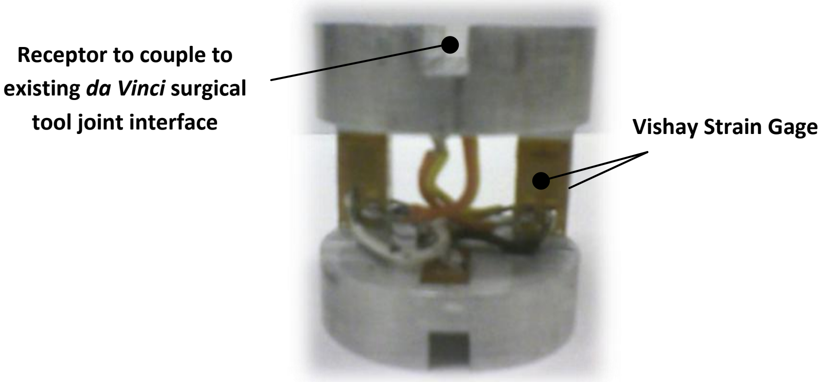
Receptor to couple to existing *da Vinci* surgical tool joint interface
Vishay Strain Gage

Figure 5.4: Aluminum sensor element with four strain gages forming a full Wheatstone bridge. The sensor is 1 inch in outside diameter.

Signal Amplifier

It was next essential to design and implement amplifiers to condition and scale the signal produced by the Wheatstone bridge. In order to be sampled with enough resolution by the analog to digital converter it was necessary to scale the signal to approximately ±2.5 volts. A gain of approximately 1000 was used. Four AD620 Instrumentation Amplifiers (Analog Devices, Norwood, MA, USA) were utilized. Trim potentiometers were utilized to zero the amplifier output. Figure 5.5 shows the connection diagram between the bridge and amplifier and Figure 5.6 shows the actual amplifier board.

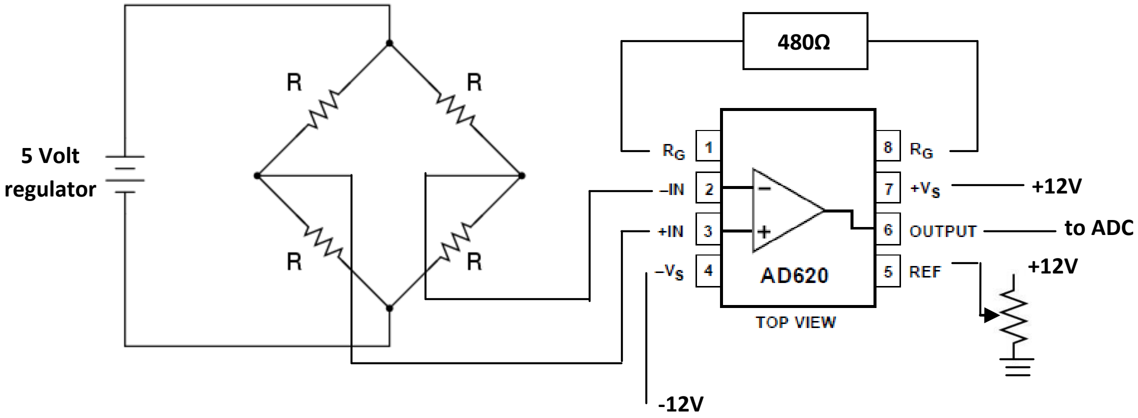

Figure 5.5: Wiring diagram for instrumentation amplifier circuit. One for each sensing element was necessary.

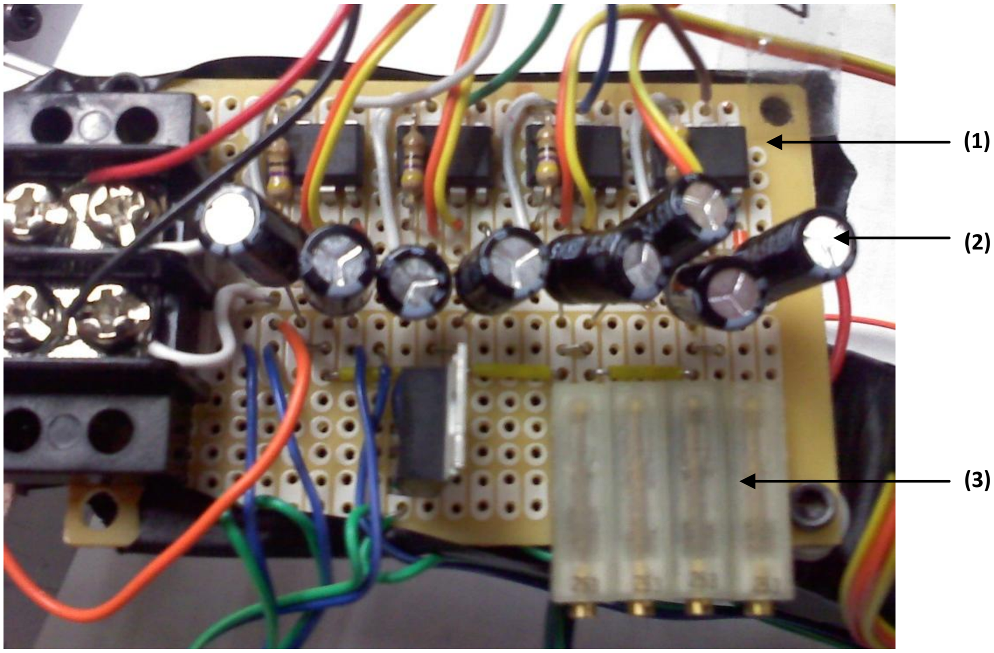

Figure 5.6: Actual signal amplifier board consisting of instrumentation amps (1) low pass filter (2) and trim potentiometers (3).

Sensor Module

A sensor module was developed to achieve several functions. First, the module was designed to hold all four sensing elements in alignment with the *da Vinci* surgical tool joints. The module allowed the sensing elements to translate vertically along their axis of rotation in order to engage and disengage the surgical tool. When the surgical tool is inserted into the sensing module, the sensing elements Figure 5.8 (11) need be translated down, preventing the elements from engaging the tool. Subsequently, when the tool is properly positioned, the elements need to advance forward and engage the tool. A plate (13 and 14) was utilized to force the sensors downward against Smalley wave springs (8 and 7) guided by steel pins (Smalley Steel Ring Company, Lake Zurich, IL, USA). Igus plastic bearings (10) (Igus, Inc, East Providence, RI, USA) were employed to enable the sensors to rotate in the direction of surgical tool joint torques.

The module was designed to fit in-between the surgical tool and *da Vinci* face plate. This space is illustrated in Figure 5.7. To properly receive the surgical tool a female receptor (12) was designed based solely on the dimensions of the surgical tool. This interface holds the tool snuggly in position, enabling the sensing elements to engage the tool. Additionally, the opposite face of this module (1) interfaces with the *da Vinci* arm faceplate, essentially mimicking the surgical tool's exact contour and connection (4). All dimensions were derived from the *da Vinci* surgical tool. The module was printed from ABS plastic using a rapid fabrication machine. Figure 5.9 shows the actual sensor module.

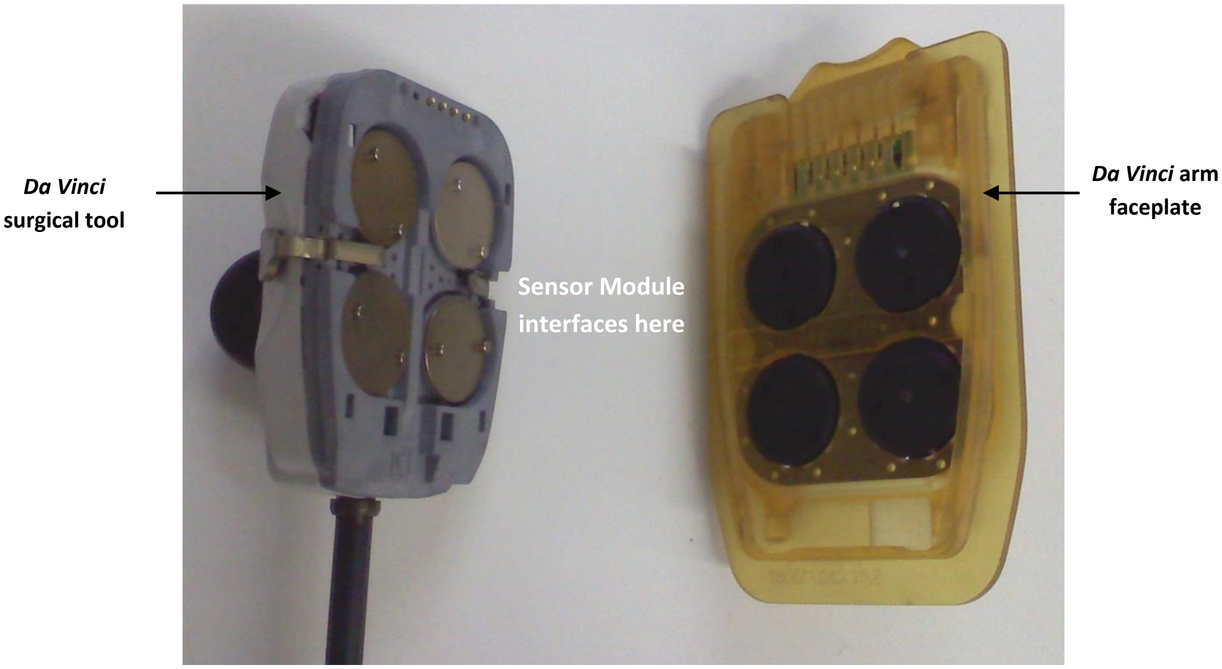

Figure 5.7: Design space for the sensor module. The device must interface with *da Vinci* arm faceplate (right) and *da Vinci* surgical tool (left).

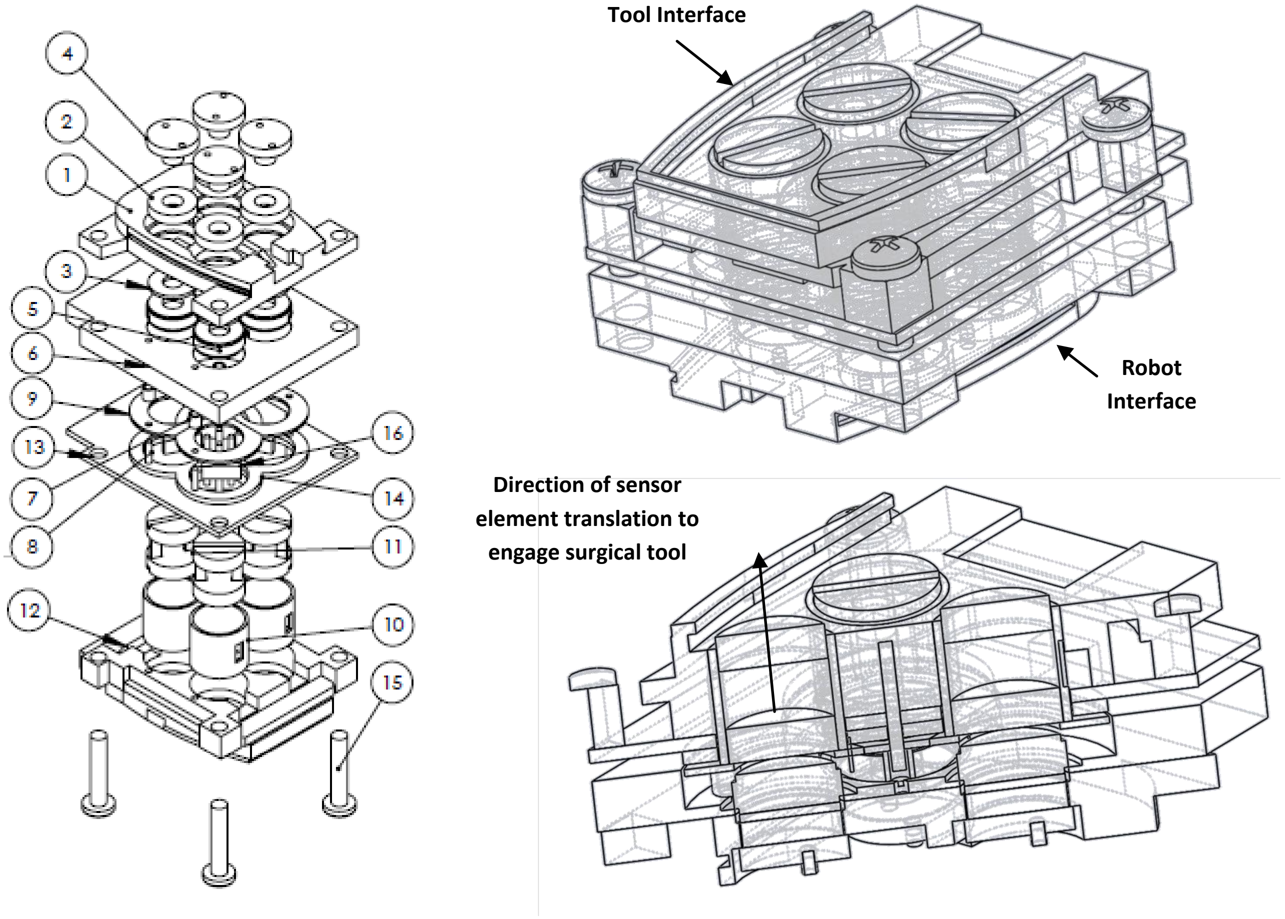

1	**Da Vinci Insert Adapter**
2	Igus Spherical Thrust Bearing Top
3	Igus Spherical Thrust Bearing Bottom
4	Male Transmission Adapter
5	Female Transmission Adapter
6	Thrust Bearing Guide
7	Smalley Wave Springs
8	Thrust Bearing Pin Guide
9	Igus Thrust Bearing
10	Igus Bearing Sleeve
11	Sensor Elements
12	End Effector Attachment Adapter
13	Sensor Height Depressor Upper
14	Sensor Height Depressor Lower
15	Transmission Pin
16	M8 x 1.25 x 40 pan head screw

Figure 5.8: Depiction of sensor module. To the left, an exploded view of module and to the right the assembled module.

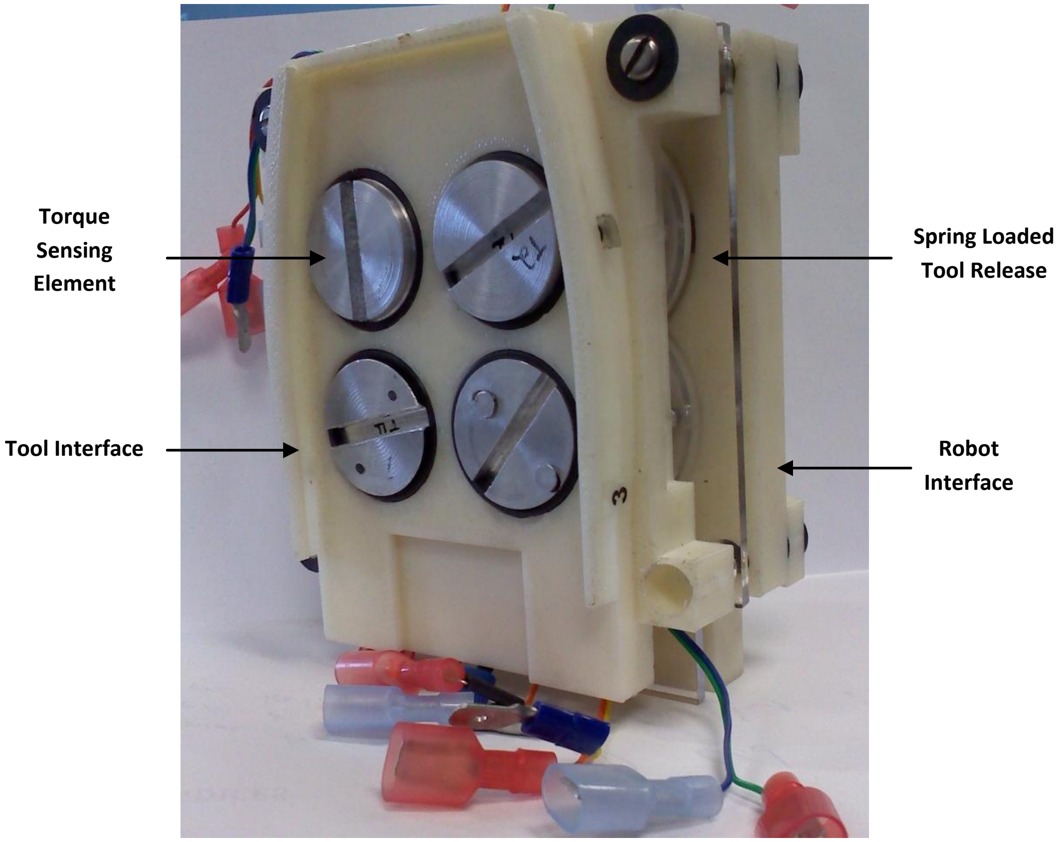

Figure 5.9: Actual sensor module.

Surgical Tool Actuator

Another subcomponent to the final design was the electromechanical mechanism to actuate and hold the *da Vinci* surgical tool. This element was critical to the research platform's functionality as it provided a way to actuate the tool's endo-wrist, a small 4 degree-of-freedom wrist at the end of the surgical tool, by means of four rotational joints at the head of the tool. To both hold and actuate the surgical tool and/or force sensing module, it was necessary for a standard *da Vinci* disposable face plate to attach to the front of this assembly. Two attachment rails were provided, see Figure 5.10. Four Faulhaber 1624S 12volt DC motors and 141:1 spur gear heads (MicroMo Electronics, Clearwater, FL, USA) were utilized as their combined torque output could simulate the torque output of the *da Vinci* during suturing operations. A custom clamp at the top of the component enabled easy mounting to the spherical wrist. The manufactured tool actuator can be seen in Figure 5.11.

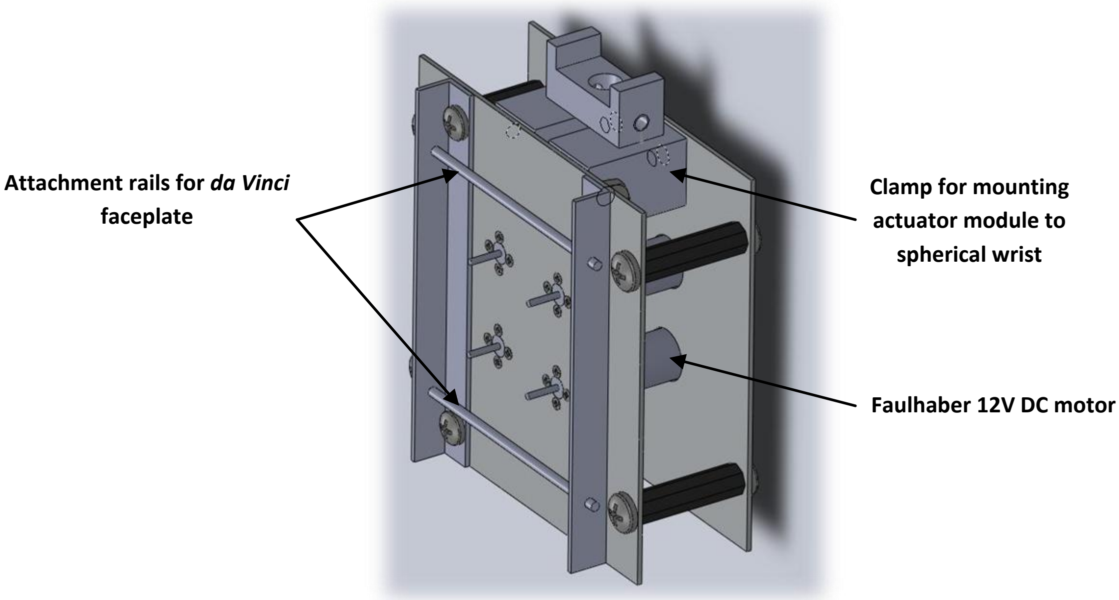
Attachment rails for *da Vinci* faceplate
Clamp for mounting actuator module to spherical wrist
Faulhaber 12V DC motor

Figure 5.10: Final surgical tool actuation module including four dc motors, an interface to the team's spherical wrist and to a standard *da Vinci* faceplate.

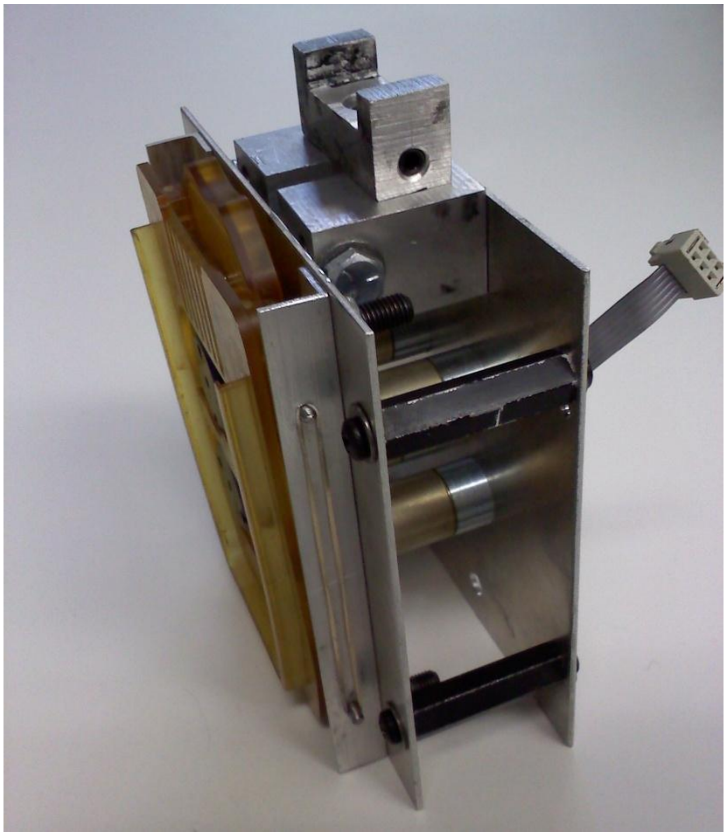

Figure 5.11: Actutal *da Vinci* surgical tool actuator

Spherical Wrist

To meet the design's functional requirements, it was necessary for the team to add 2 additional degrees-of-freedom to the 4 degree-of-freedom SCARA robot currently available and serving as the backbone of the research platform. It was intended for these two additional degrees-of-freedom to merge with the final axis on the robot. This would create 3 axes whose actuating axis all intersect at a single point, creating a spherical wrist capable of specifying the tool's orientation. The schematic representation of a spherical wrist can be viewed in Figure 5.12.

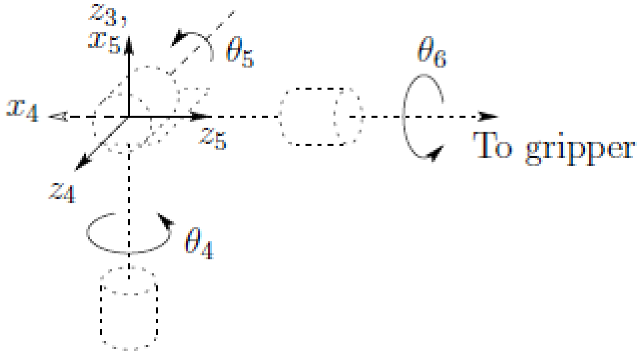

Figure 5.12: Illustration of the final three axes forming a spherical wrist. Two of these three axes are provided by the team's custom spherical joint.[1]

Inspiration for the mechanical design of the spherical wrist came from a previous project of the design team's advisor. The original mechanism was used to emulate eye movement. Each actuator, or DC motor, articulates a single semicircular tool guide. These guides are oriented perpendicular to one another, ensuring independent control of rotations about a fixed point. A plastic ball is used as a bearing surface, allowing the tool to move freely with the guides. See Figure 5.13.

[1] (Spong, Hutchinson and M)

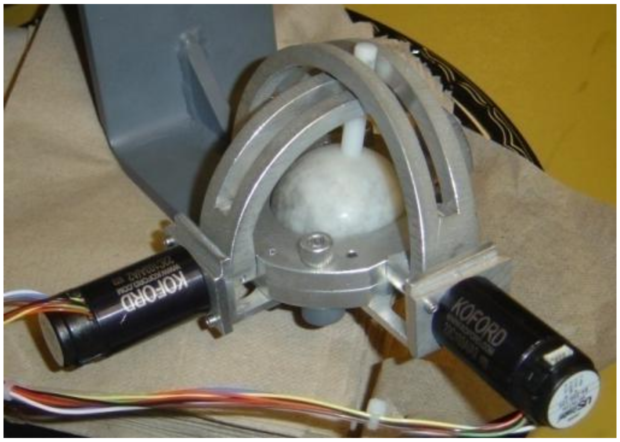

Figure 5.13: Inspiration for the design of the spherical wrist came from a device to emulate eye movement.

The final spherical wrist was printed from ABS plastic using a rapid prototyping 3D printer. Because of the material's limited strength, careful consideration was taken to make the semispherical guides (shown in Figure 5.14 (1)) thick enough, preventing deflection under operational load. Two iterations of the wrist were necessary in order to indentify this and other problems. For instance, because of the resolution of the rapid prototyping machine, metal bushings and steel shafts were used to construct the guide joints (2). The nylon ball in the center (3) was held in place by a removable plate, allowing the wrist to be easily assembled and disassembled. Two 12V DC Globe Motors and shaft encoders (4) (Globe Motors Inc, Dayton, OH, USA) were utilized to actuate each guide and measure angular displacement. The assembled spherical wrist can be seen in Figure 5.15.

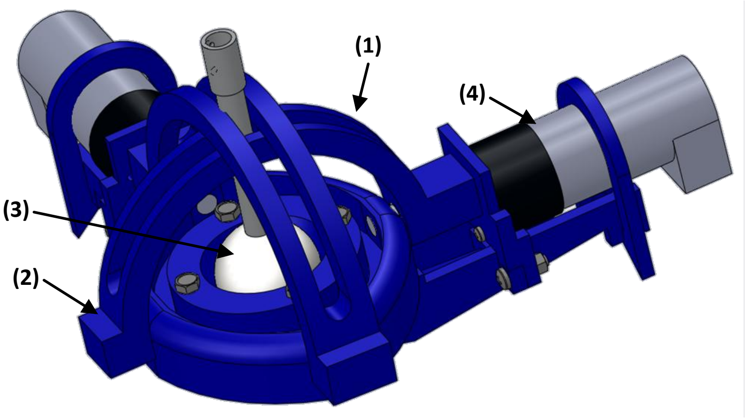

Figure 5.14 Final design of spherical wrist used to orient *da Vinci* surgical tool.

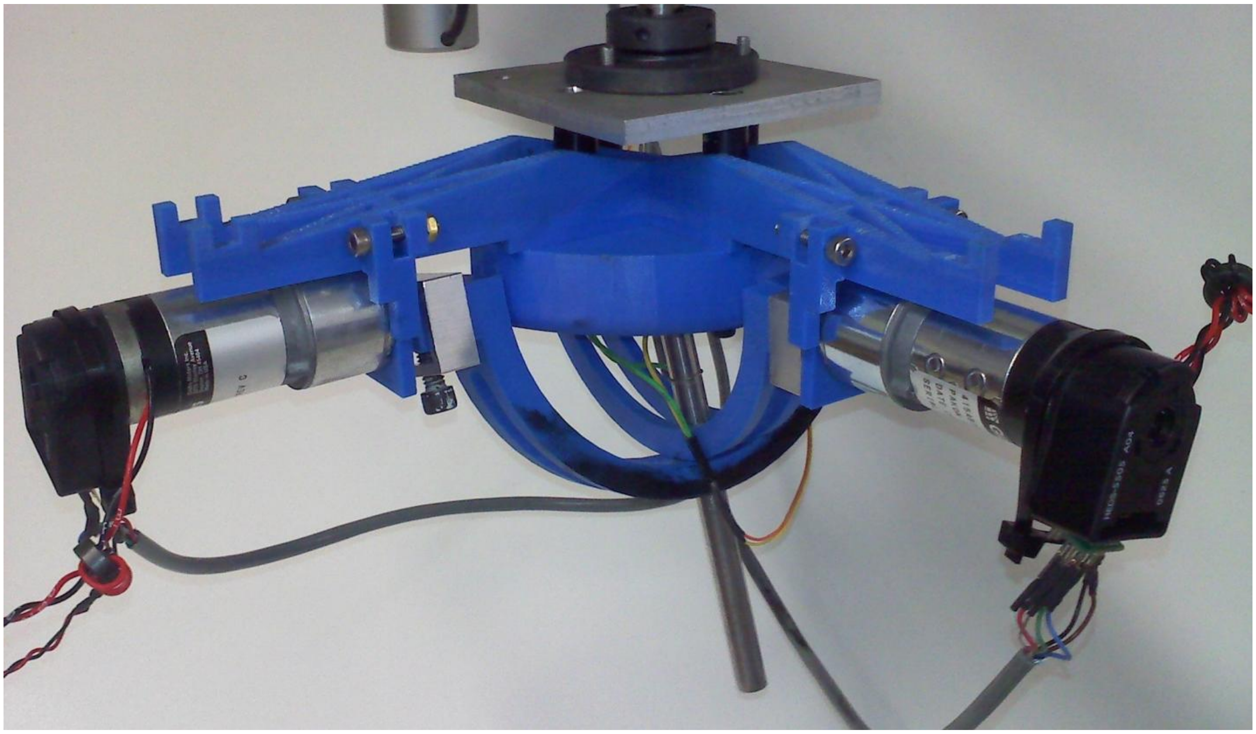

Figure 5.15 Actual implementation of spherical wrist final design.

SCARA Robot and Kinematic Models

In order to achieve proper control over the robot, the robot's joints, physical dimensions, and coordinate frames had to be modeled using forward kinematics. Subsequently, in order to specify the robot's Cartesian position and orientation based on joint positions (variables under control), the inverse kinematics of the 6 degree-of-freedom manipulator were solved.

Initially, coordinate frames, joint angles, link lengths and offsets were defined. These definitions are illustrated in Figure 5.16. Using this model, Denavit-Hartenberg (D-H) parameters were specified and used to generate the robot's forward kinematics. These parameters are shown in Table 5.1. Individual coordinate frame transformations were made, T_i^{i+1}. Total coordinate transformation between the base coordinate frame F_0 and the tip coordinate frame F_6 was determined by cascading the individual transformations, $T_0^6 = T_0^1 T_1^2 T_2^3 T_3^4 T_4^5 T_5^6$.

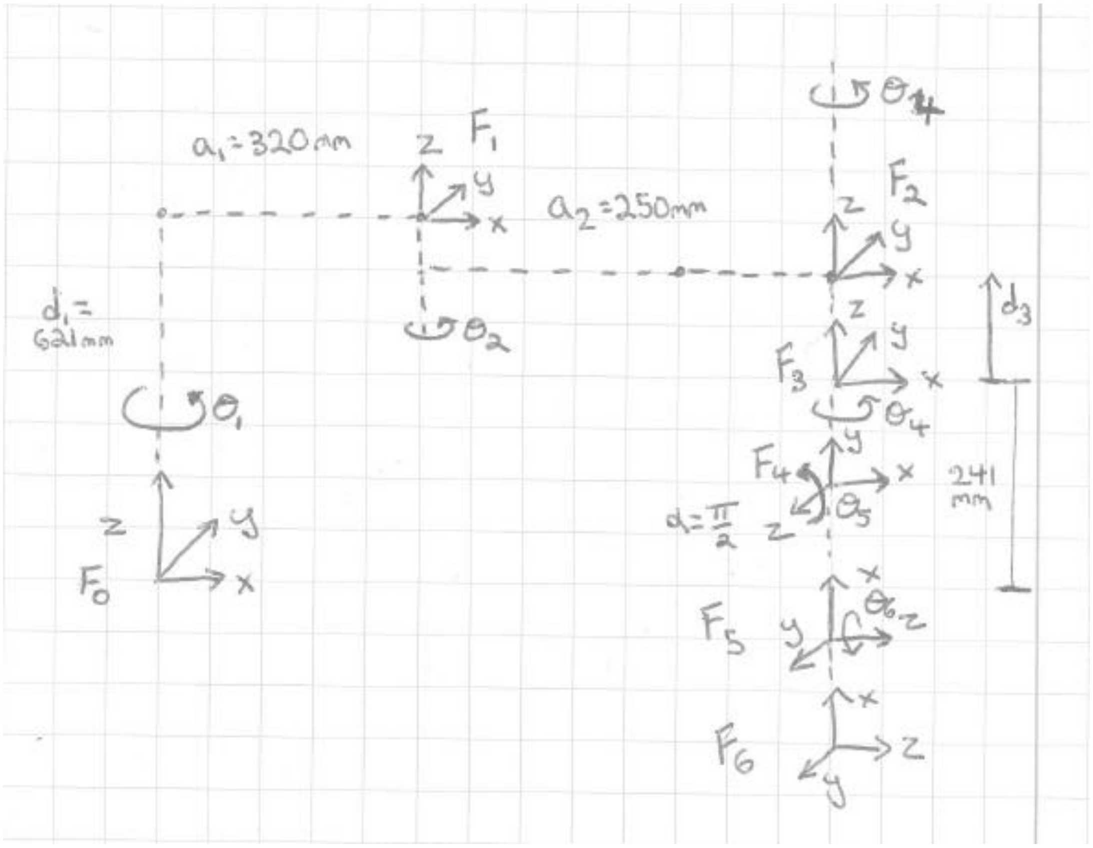

Figure 5.16: Coordinate frame definitions, assumed offsets, link lengths, and joint angle directions for the full 6 DOF robot.

Table 5.1: Corresponding D-H parameter list for full 6 DOF robot, all dimensions in millimeters.

Link	Rot_Z	$Trans_Z$	$Trans_X$	Rot_X
Link 1	θ_1	621	350	0
Link 2	θ_2	0	250	0
Link 3	0	$d_3 - 241$	0	0
Link 4	θ_4	0	0	$\pi/2$
Link 5	$\theta_5 + \pi/2$	0	0	$\pi/2$
Link 6	θ_6	0	0	0

To confirm the kinematic model's accuracy, a Matlab simulation (The MathWorks, Inc, Natick, MA, USA) was created to visually plot the robot in 3D space. The simulation inputs were joint angles and its output was the pose and orientation of the robot. Figure 5.17 details the simulation's output.

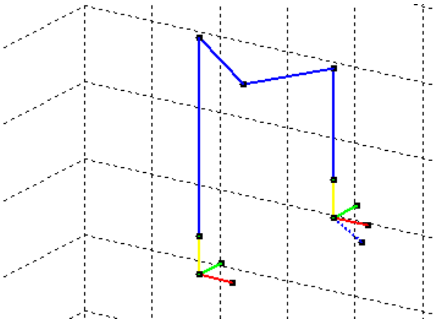

Figure 5.17: Matlab simulation of Forward robot kinematics

Inverse kinematics were necessary to determine joint angles from a given Cartesian pose. Inverse kinematics were determined through geometry. Knowing the geometry of the robot, joint angles theta one and theta two were solved for in terms of a specified point **(P_x, P_y, P_z)**. Note the translation of **d_3** directly maps to **P_z** so the calculation is intentionally overlooked in the process below.

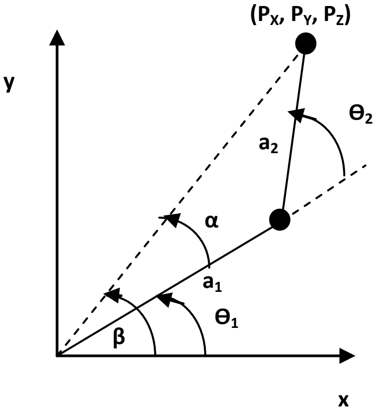

Figure 5.18: Geometric layout of robot arm used inverse kinematics

Using the law of cosines, theta two was first solved for:

$$\Theta_2 = cos^{-1}\frac{\left(P_x^2 + P_y^2\right) - \left(a_1^2 + a_2^2\right)}{2a_1a_2}$$

In a similar manner, Alpha and Beta were subsequently found:

$$\alpha = cos^{-1}\frac{a_1^2 + P_x^2 + P_y^2 - a_2^2}{2a_1\sqrt{P_x^2 + P_y^2}}$$

$$\beta = \tan^{-1}\frac{P_y}{P_x}$$

The inverse orientation kinematics, specifying the tool's orientation in 3D space, were found by simple geometry. Here, theta five and theta six are the result from specifying a unit vector, the tool's approach vector.

$$\Theta_5 = \tan^{-1}\frac{Ox}{Oz}$$

$$\Theta_6 = \tan^{-1}\frac{Oy}{Oz}$$

One of the major design objectives outlined in the previous chapters was the establishment of a remote center of motion about an arbitrarily fixed point in space. The concept of a tool being articulated about a remote center is illustrated in Figure 5.20.

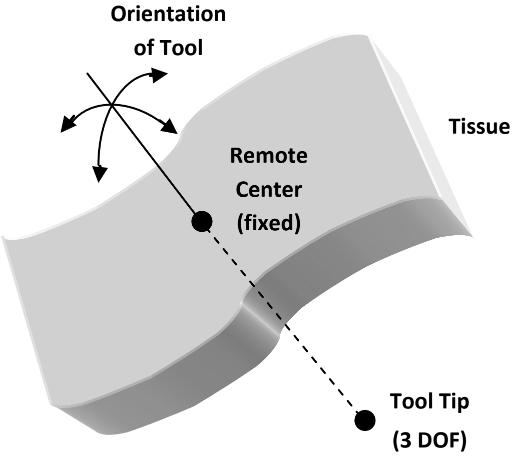

Figure 5.20: Articulation of a tool about a fixed remote center

In conjunction with the user's desired input of the 3D Cartesian end-effecter position and fixed tool length, the remote center will constrain all 6 degrees-of-freedom available on the research platform. The end-effecter position and remote center together form a line. This line specifies the tool orientation through a unique unit vector. Based on the tool's orientation and internal and external lengths, the robot's wrist position is determined. Here, ***i*** denotes user input, ***r*** : remote center (***Rc***), ***Ti*** *:* the tool's internal length, ***To*** : the tool's external length, ***u***: the tool's unit vector, and **P** : the robot's wrist position. The remote center calculations are depicted in Figure 5.20.

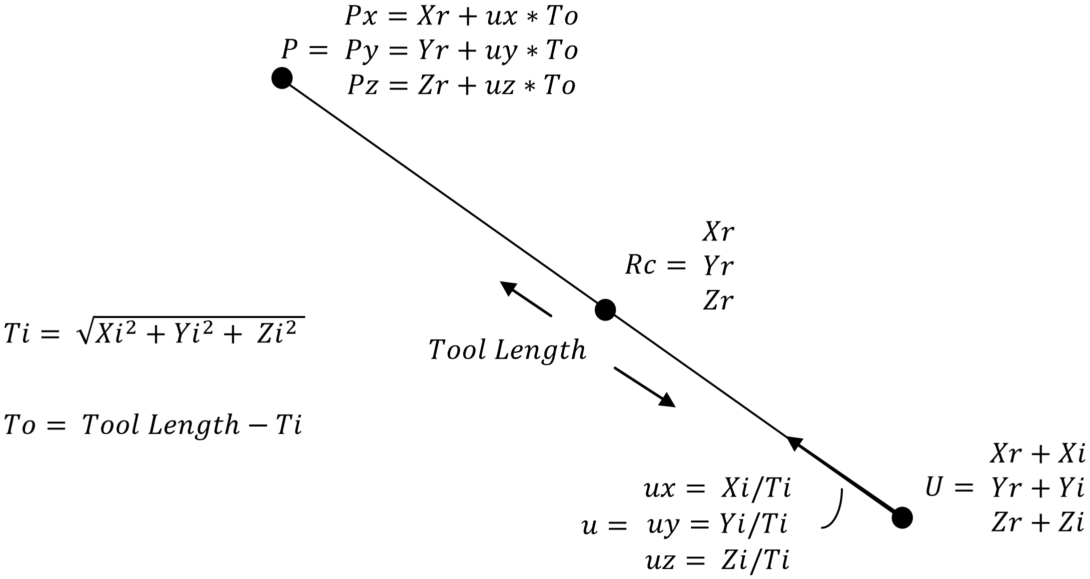

$$P = \begin{matrix} Px = Xr + ux * To \\ Py = Yr + uy * To \\ Pz = Zr + uz * To \end{matrix}$$

$$Rc = \begin{matrix} Xr \\ Yr \\ Zr \end{matrix}$$

$$Ti = \sqrt{Xi^2 + Yi^2 + Zi^2}$$

$$To = Tool\ Length - Ti$$

$$U = \begin{matrix} Xr + Xi \\ Yr + Yi \\ Zr + Zi \end{matrix}$$

$$u = \begin{matrix} ux = Xi/Ti \\ uy = Yi/Ti \\ uz = Zi/Ti \end{matrix}$$

Figure 5.20: Depiction of tool and arbitrarily placed remote center of motion. These calculations were run in real-time to solve for the position and orientation of the robot's wrist.

Implementation and Synthesis of Robot

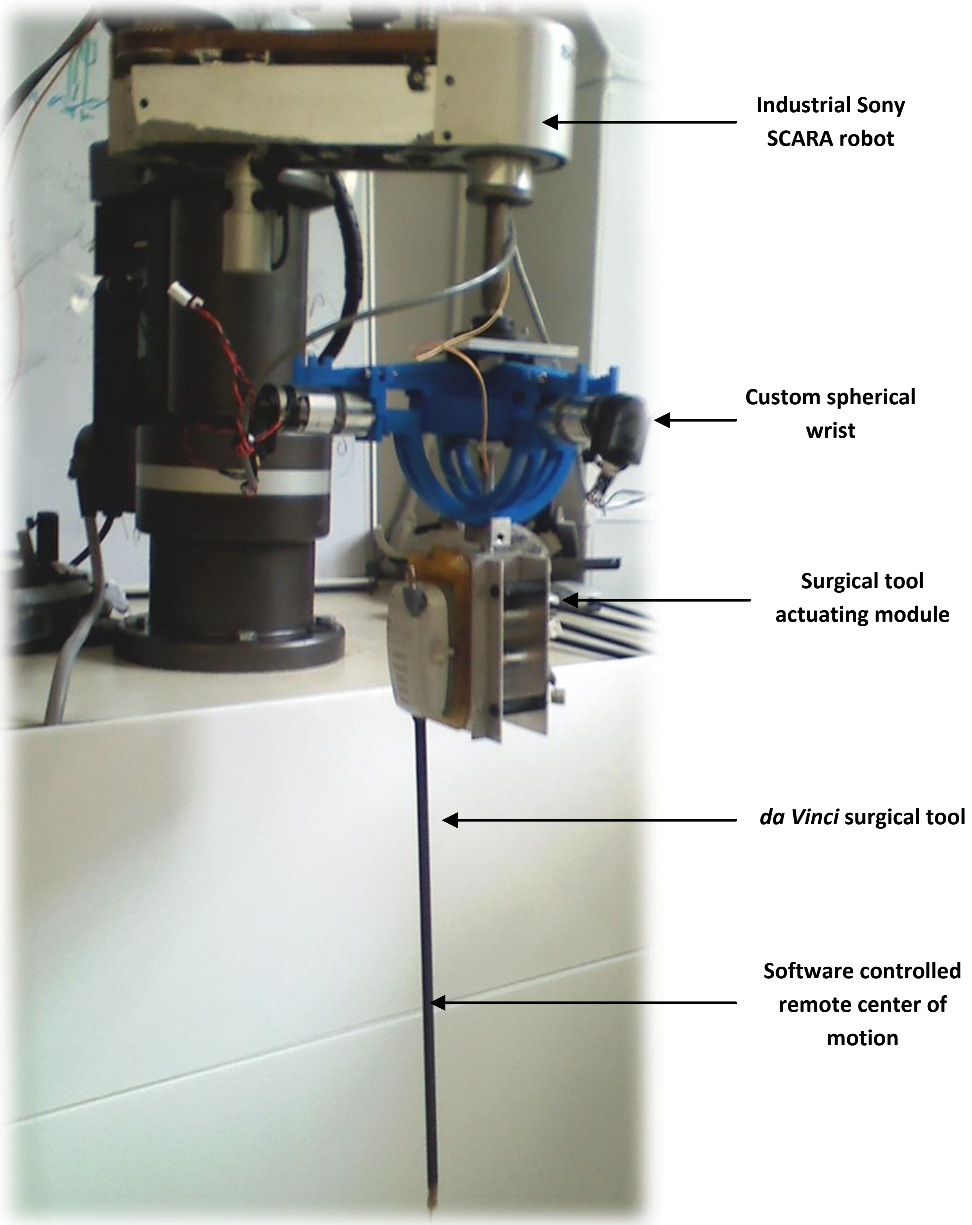
Industrial Sony SCARA robot
Custom spherical wrist
Surgical tool actuating module
da Vinci surgical tool
Software controlled remote center of motion

Figure 5.21: Synthesis of the previously described subcomponents: Sony SCARA industrial robot, spherical wrist, tool actuating module, torque sensing elements and force sensor module, and surgical tool.

The Sony SCARA robot, custom spherical wrist, surgical tool actuating module, force sensing elements and module, as well as the surgical tool were all integrated and implemented. Figure 5.21 depicts the synthesis of these major subcomponents.

Robot Controller Hardware and Software

Hardware

In order to actuate the robot, command signals were generated by digital to analog converts (DACs) on both the Poseidon embedded computer and Ruby-MM-4 analog output module (Diamond Systems, Mountain View, CA, USA). These DACs were arranged in a bipolar configuration (±10 volts) and have 12 bits of resolution. A simple program was provided by Diamond Systems to interface with the DACs. Base address, output range, and calibration options were set using onboard jumpers.

Because of the DC motors present on both the spherical wrist and industrial manipulator, the command signals needed to be amplified. 6 LDH-S3 linear amplifiers (Western Servo Design, Carson City, NV, USA) were utilized. These amplifiers were configured in a bipolar arrangement and could source up to 2 amps continuous and 5 amps peak. Using analog potentiometers located on each amplifier board, the amplifiers were zeroed and subsequently the gain was adjusted such that the ±10V DAC signal was scaled to ±12 volts, the voltage required to run the DC motors. Additionally, a potentiometer was provided to adjust the time constant of the amplifier, this was not used due the robot's high inertia load. Figure 5.22 illustrates the amplifiers used.

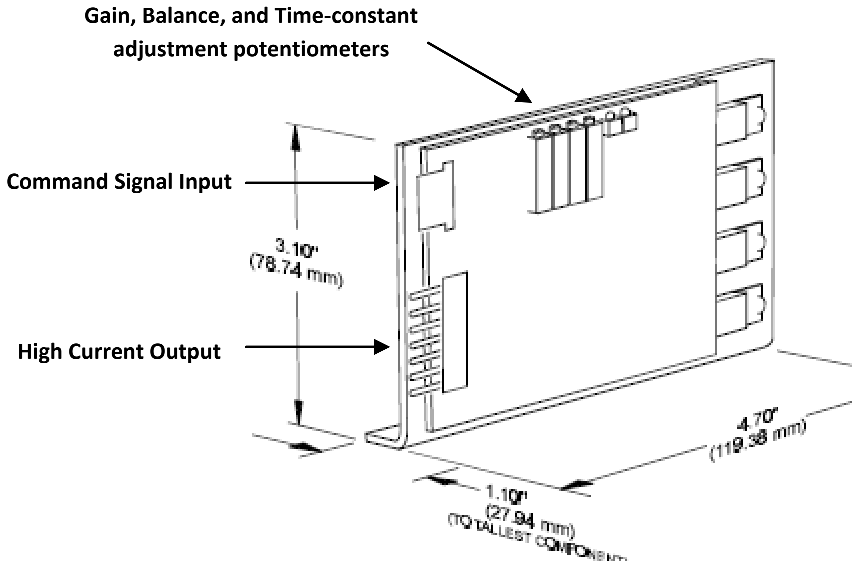
Gain, Balance, and Time-constant adjustment potentiometers
Command Signal Input
High Current Output
3.10" (78.74 mm)
4.70" (119.38 mm)
1.10" (27.94 mm) (TO TALLEST COMPONENT)

Figure 5.22: LDH-S3 Linear Amplifiers used amplifier control signals and control DC motors. Figure adapted from Western Servo Design, Carson City, NV, USA

In order to interpret quadrature encoder signals coming from both the industrial manipulator and the spherical wrist, a hierarchical interface was developed. 6 LS7366 32-bit quadrature counters with serial interfaces (LSI/CSI, Melville, NY, USA) were used to capture and count the quadrature signals coming from rotary encoders at each axis. An Atmega 644P microcontroller (ATMEL Corporation, San

Jose, CA, USA) was used to interface with each positional encoder. This single microcontroller was responsible for writing a read request (via 4 wire serial) and subsequently reading the 32-bit position count from each of the 6 integrated circuits.

Using an FTDI USB to serial communication chip (Future Technology Devices International Ltd, Glasgow, UK), reliable communication was established between the low level Atmega microcontroller (TTL serial) and the embedded Linux computer (USB 2.0). The highest level controller, the embedded Linux system, sends a read request to the Atmega microcontroller and subsequently reads 16 bytes of data. Each joint position consists of 2 bytes and there are 4 additional bytes used to check the strings beginning and end locations, as the data is sent sequentially joint by joint. The hierarchal structure of this process is depicted in Figure 5.23.

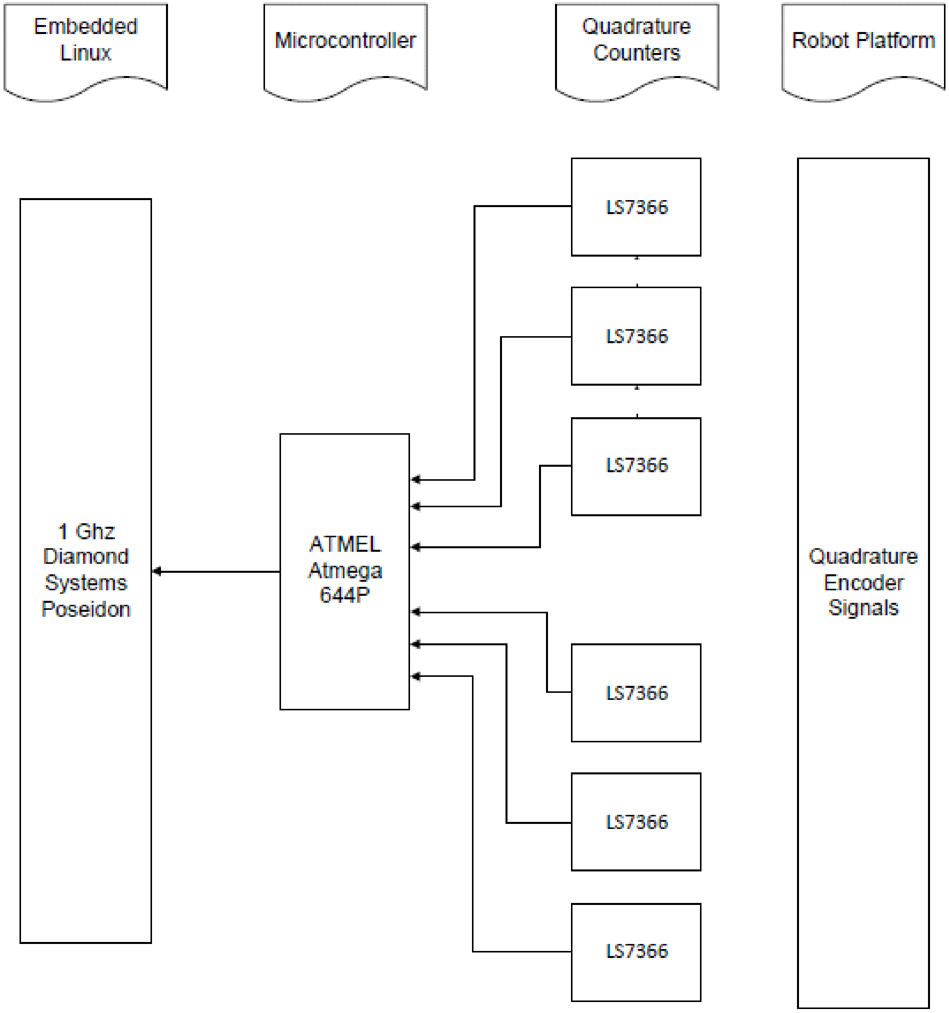

Figure 5.23: Flow of positional data from robot to highest level control process. Steps include quadrature counter ICs, microcontroller, and embedded Linux processor.

Software

The control process was written in C code in Linux User Space. The control process handles all interaction with peripherals as well as the kinematics calculations. After the process is initialized, it reads a packet of previously requested joint positions waiting in the serial buffer (read request is sent during the previous execution of the control loop). Subsequently, joint torques are sampled from the sensor module using the Poseidon's ADCs. Representative Cartesian forces are determined and written to a named shared memory allocation. A separate user space process, the Novint Falcon control code, reads the shared memory allocation as soon as a synchronization semaphore has been allocated, indicating the control process has finished writing the force structure to the memory location. In turn, the falcon writes positional data from the user into a separate shared memory allocation before it is blocked by the unavailability of the semaphore. Because of this, the control process is able to access the positional data just prior to releasing the blocked falcon process.

The control process continues to compute the necessary joint angles to achieve the user's specified Cartesian pose by means of inverse kinematics. Once desired joint angles are determined, errors between the previously read actual angles and the desired joint angles are determined. A PID control loop attempts to converge these errors to zero and results in 6 independent control signals. Control signals are written to the Ruby-MM-4 DAC module. Finally, the control process blocks until a binary semaphore resource (handled by the Kernel) becomes available.

The Kernel allocates the mention binary semaphore every 1 ms. The control process is essentially put to sleep until the resource becomes available. The kernel module takes advantage of the RTAI kernel patch, utilizing a HAL (hardware abstraction layer) to achieve true real-time operation independent of user space processes.

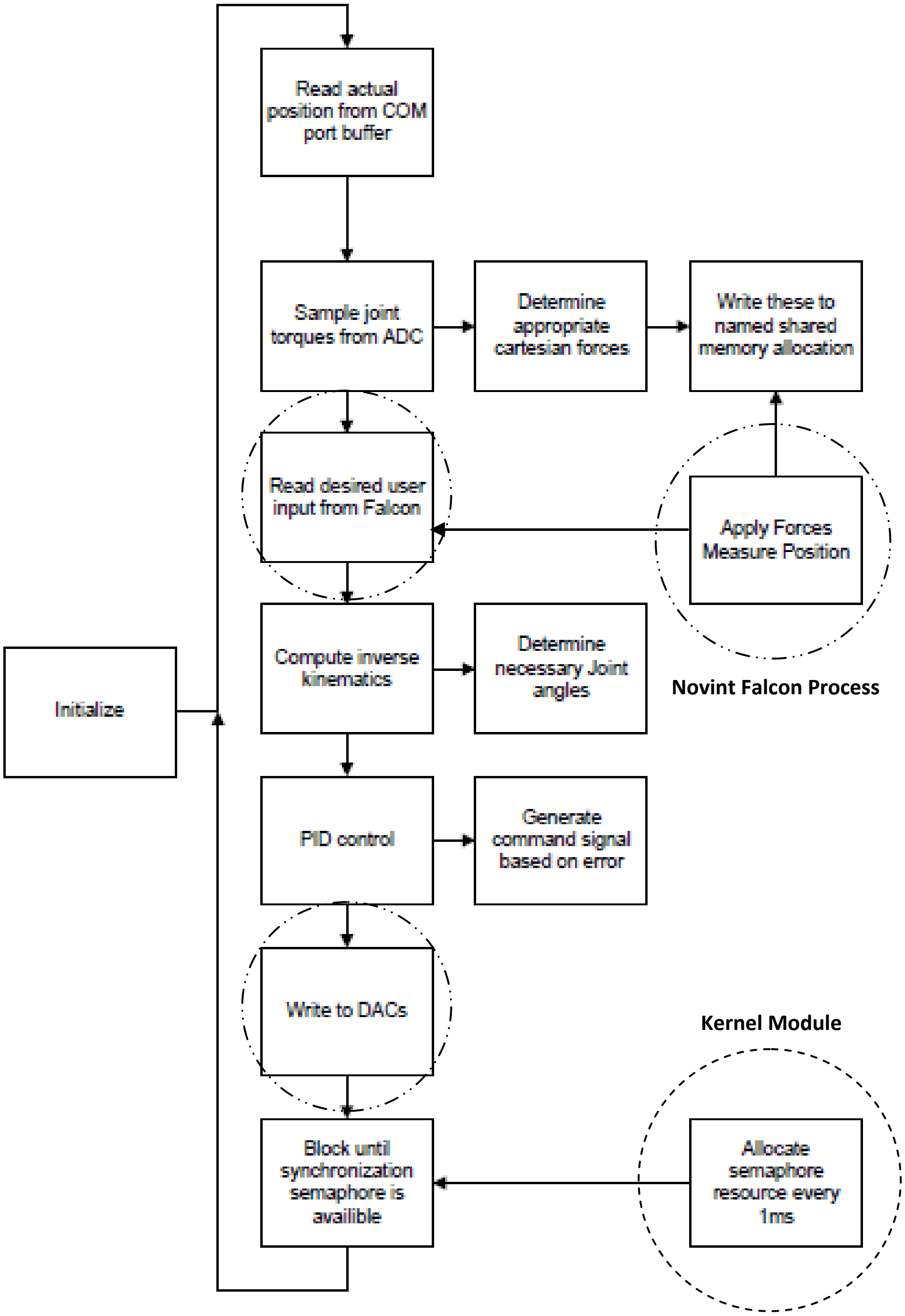
Read actual position from COM port buffer
Sample joint torques from ADC
Determine appropriate cartesian forces
Write these to named shared memory allocation
Read desired user input from Falcon
Apply Forces Measure Position
Novint Falcon Process
Initialize
Compute inverse kinematics
Determine necessary Joint angles
PID control
Generate command signal based on error
Write to DACs
Kernel Module
Block until synchronization semaphore is availible
Allocate semaphore resource every 1ms

Figure 5.24: Flow of control process. The responsibilities of the control process as well as the peripherals and processes it interacts with.

User Haptic Interface

In order to provide haptic sensation to the user, a Novint Falcon haptic game controller (Novint, Albuquerque, NM, USA) was used. This device not only allowed the position of the user's hand to be captured but also for forces to be transmitted to the user's hand. In order to interface with the Falcon, an open-source driver was utilized as there are no Linux drivers provided by the manufacturer. Considerable time was spent compiling and implementing the driver. A separate process was used to control the Falcon. This object oriented program read position data from the Falcon, computed forward parallel robot kinematics to determine end effect position, and also applied specified Cartesian forces. The design team's control process interfaced with the Falcon's process through the introduction of named shared memory allocations. The control process wrote force data to a memory address for the Falcon process to read, and likewise the Falcon process wrote positional data to a memory address for the control process to read. Inter process communication was synchronized, again, through the use of binary semaphores. This ensured memory was not accessed by multiple processes at the same time.

Control System Implementation

The final control system design was built and programmed. Figure 5.25 details the system integration.

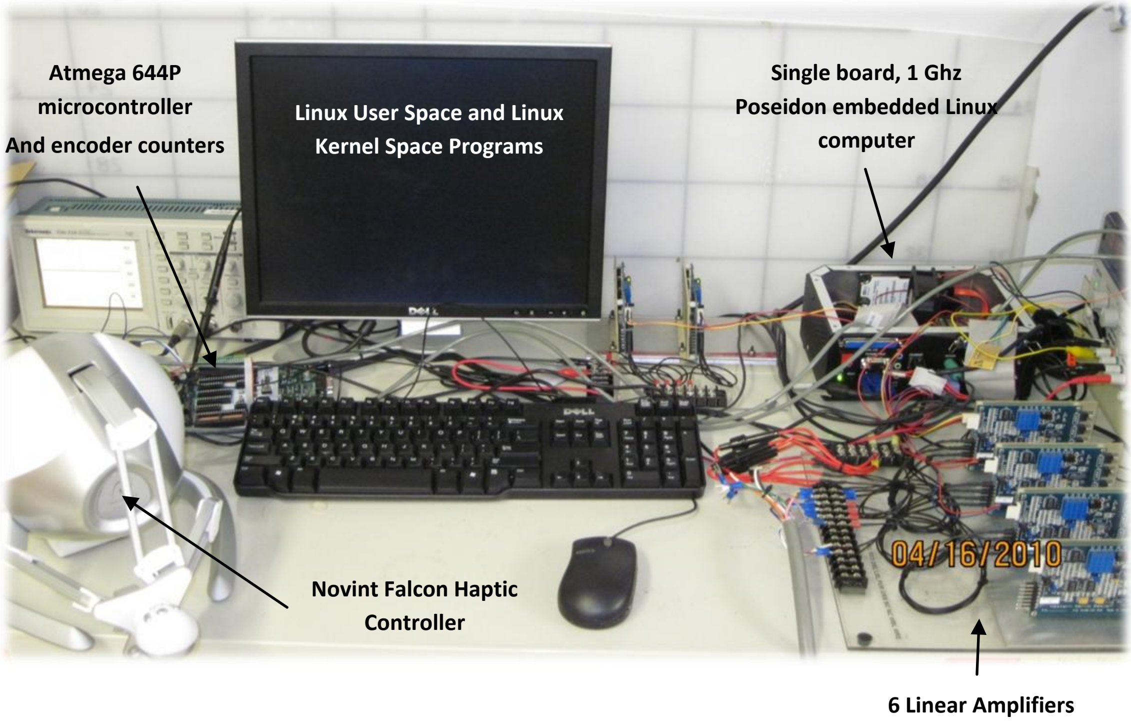

Figure 5.25: Developed a complete robot control system with real-time Linux PC, custom high-speed encoder interface, amplifier modules, and haptic interface.

6. FINAL DESIGN VALIDATION

Several steps were taken by the design team to verify the devices functionality. In order to validate the sensor module the team brought the subsystem to Children's Hospital Boston, where Dr. Hiep T. Nguyen allowed testing on an actual *da Vinci* Surgical System. The team fit the sensing module on the robot and it successfully fit between the arm's faceplate and the surgical tool. Figure 6.1 shows the module fitting on the actual *da Vinci* surgical robot. It is important to note that this was the primary objective of the sensing module; it must fit on the existing *da Vinci* device and hold the surgical tool. This design objective was indeed accomplished.

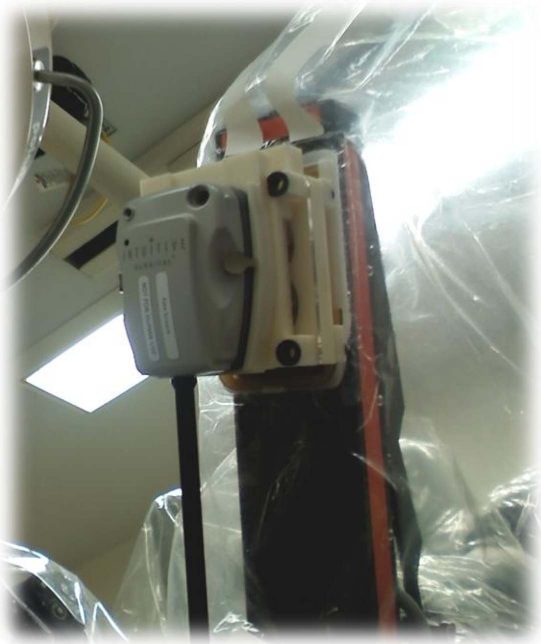

Figure 2.1: Sensor module on da Vinci Surgical robot at Children's Hospital Boston, confirming design objective

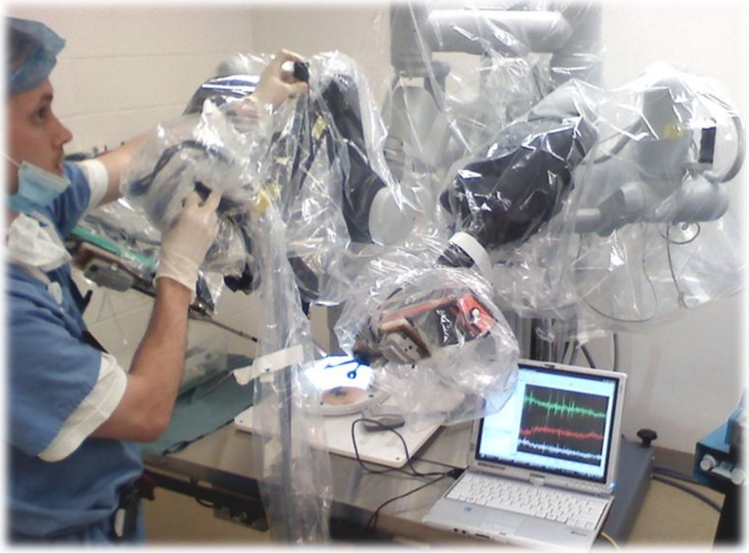

Figure 6.2: Further confirmation of device functionality, the arm was moved while the sensor module was attached.

Additionally, it was required that the force sensing module measure joint torques reliably with repeatability. In order to confirm this objective sensor elements were individually calibrated. The design team examined the calibrations' linearity (the linear relationship between applied torque and sensor signal after amplification using the designed amplifier module). Each sensor element showed extremely high calibration linearity, with an $R^2 = 0.99$. The calibration was performed by first fixing one end of the sensing element to ground. Next, several precise weights were hung at a controlled distance. Applied torque was calculated and sensor amplifier output was recorded at each applied torque. The experimental set up for calibration procedures is shown in Figure 6.3. Curves and trend lines were plotted using Microsoft Excel. Figure 6.4 illustrates the results of a sensor element calibration.

The minimal variance between sensor elements speaks to the repeatability of our methodical approach. The high linearity confirms the theoretical calculations and design of our sensing element. The design successfully met the objective of measuring tool interaction forces.

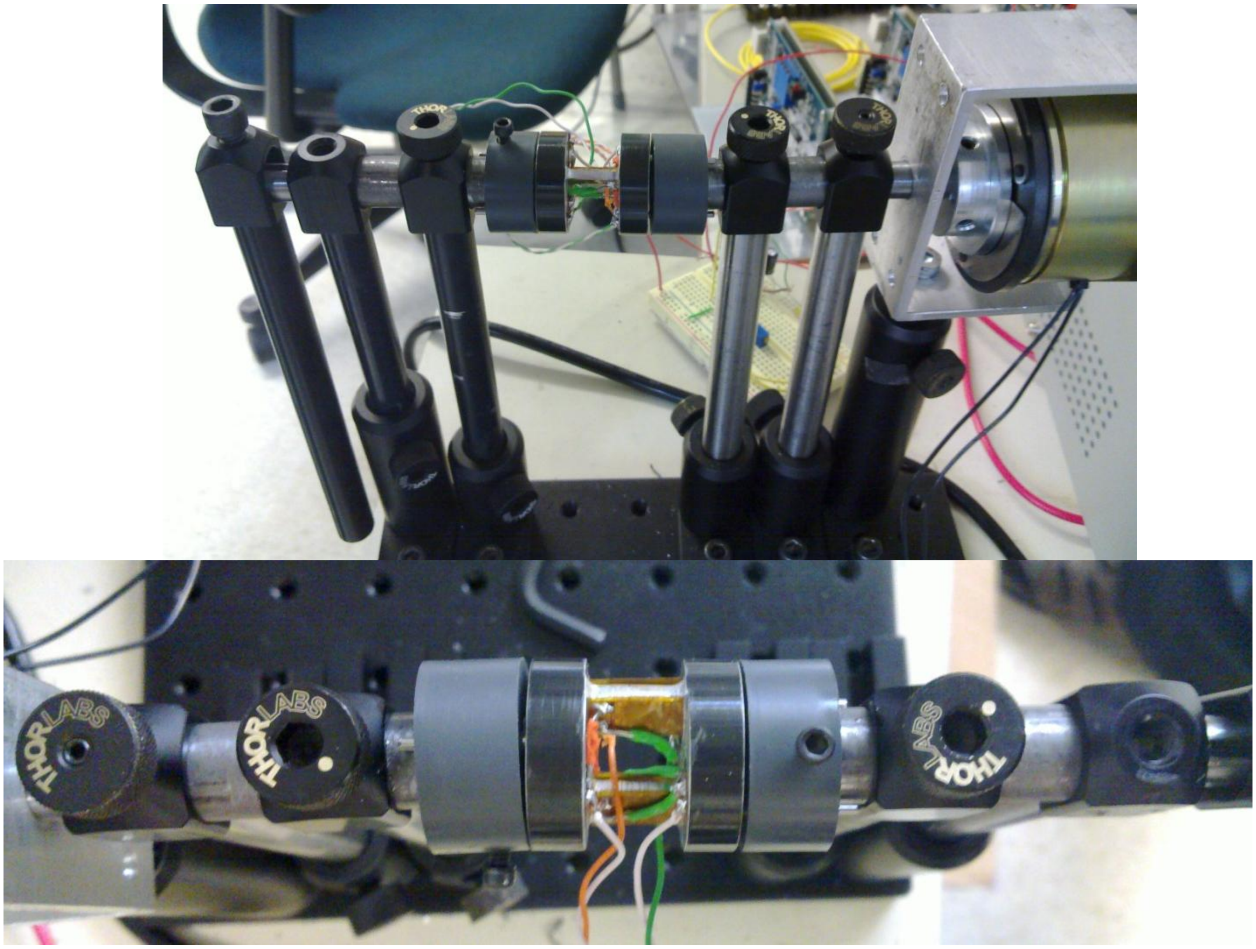

Figure 6.3: Test rig used to calibrate sensing elements. A magnetic clutch prevented one end of the sensor from rotating while a load was systematically applied to the opposite end. Applied torque was calculated and amplified voltage output recorded.

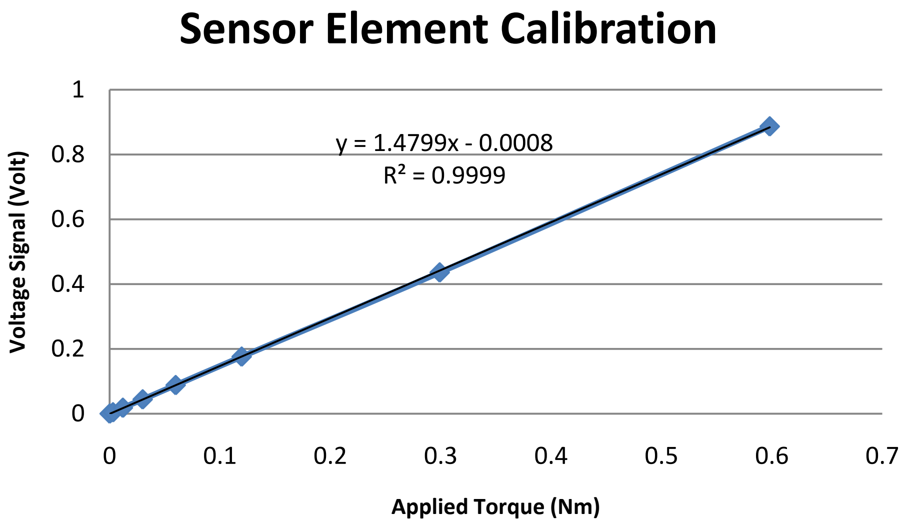

Figure 6.4: The linearity calibration result for 1 of the 4 custom-made torque sensors that couple between the surgical tools and the *da Vinci* robot.

Lastly, the design team confirmed the kinematic positioning of the robotic platform about a remote center. Through multiple demonstrations, it was confirmed that the platform successfully and reliably interpreted user input from the Novint Falcon, utilized this positional information to dictate tool-tip position and maintained a remote center of motion at a simulated patient-machine interface. Figure 6.5 illustrates the user inputting a desired tool-tip position and the robot achieving that tip position while orienting the tool to maintain a remote center of motion.

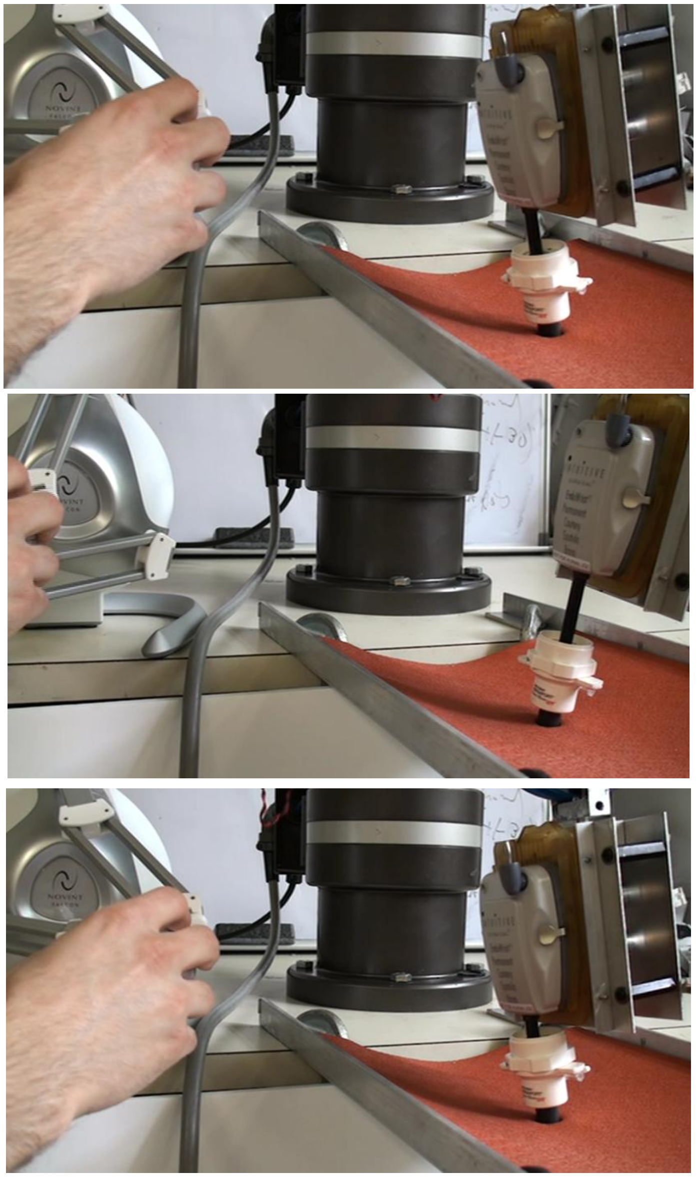

Figure 6.5: Design verification of robots ability to maintain remote center of motion while interpreting user input for end effecter positioning.

Perhaps the greatest testament to the project’s success was the system wide integration of the team’s developed subcomponents. The complex synergy arising from integrating multiple subcomponents can often leave the final product in a non-functional state. Here, the haptic user interface, robot control system (software and electronics), the custom spherical, tool actuator, and sensor module all integrate into a solid research platform. Figure 6.6 details the final system wide integration on the robot’s final design.

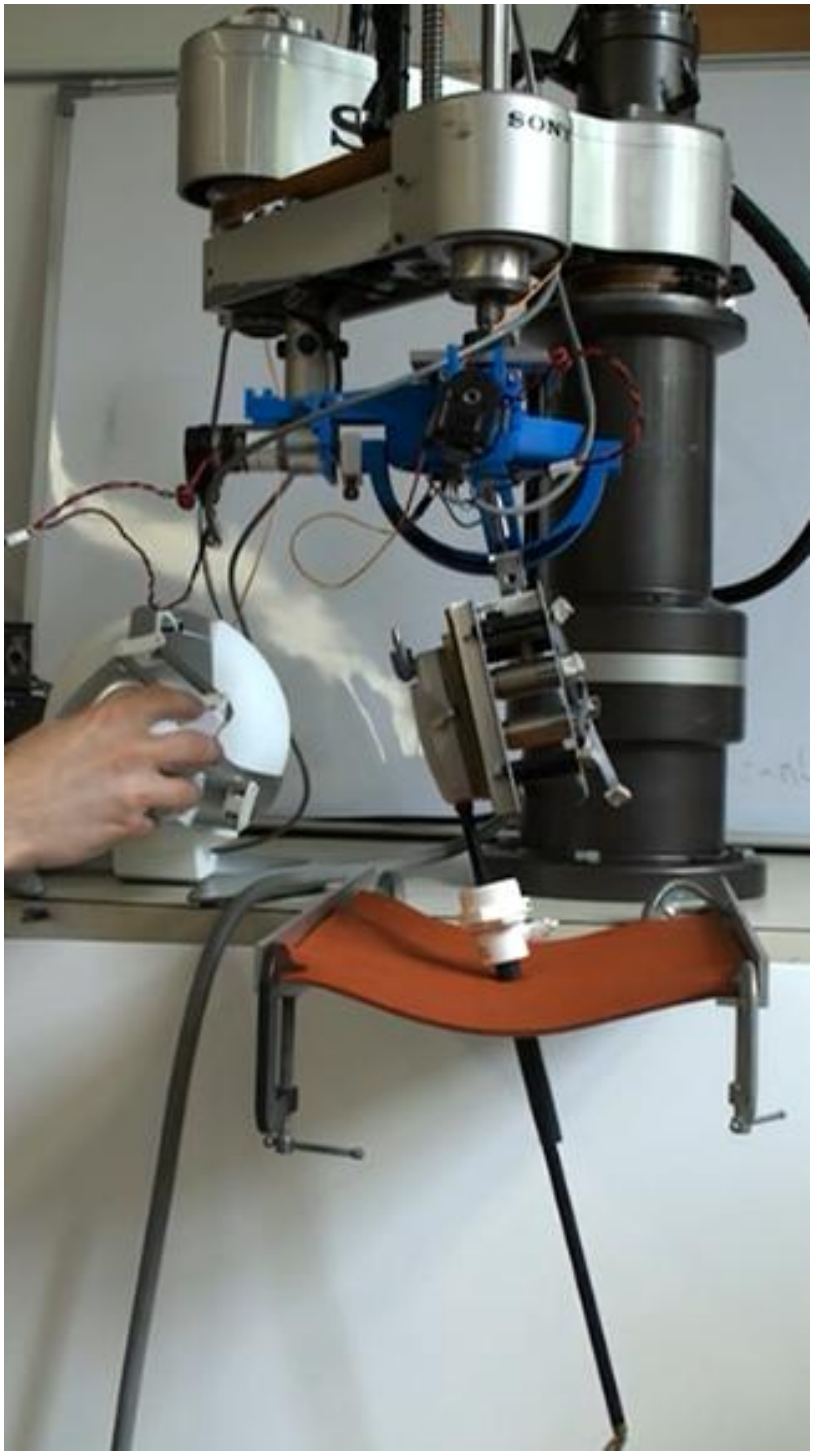

Figure 6.6: Final design implementation. A major objective of the project was successful system wide integration of the research platform

7. DISCUSSION

Several accomplishments are worth elaborating on from the research team's work. Concisely the team successfully:

- Created a simulated *da Vinci* arm using an industrial robot, custom spherical wrist, and a surgical tool actuator module.
- Developed a custom Linux-based control system and high speed encoder interface for the robotic platform.
- Developed a torque sensing module that interfaces between *da Vinci* surgical tools and the robot's arm (real *da Vinci* or our simulator) to measure tool-tissue interaction forces.
- Implemented inverse kinematics control of the robot with virtual remote center of motion using a haptic feedback input device.

A *da Vinci* arm's functionality was properly reproduced. Although the *da Vinci* uses a mechanical remote center of motion, the research team was able to employ a software remote center of motion to achieve the same functionality. Although the design was only required to hold a remote center that would minimize skin stretch at the point of entry into the patient, confirmation as to the accuracy of the remote center and the tool tip position should be externally measured. The design team suggests the use of fiducially tracking beads on both the remote center of motion and the end effecter tip to quantify tool positioning errors. However, the team did attempt to minimize joint space errors. Figure 7.1 depicts the desired and actual joint position of one of the robot's 6 joints. Control parameters were tuned until error was minimized.

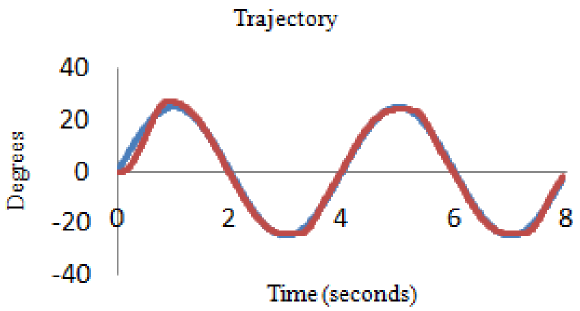

Figure 3.1: Desired vs. actual trajectory of one of the robot's joints.

The robot's spherical wrist was able to orient the surgical tool and integrate onto the existing industrial manipulator. It was determined that, although there is room for both mechanical and electric optimizations of this subcomponent, it met the functional requirements of the design and easily provided two additional independent degrees-of-freedom.

Furthermore, the custom surgical tool actuator module was able to mount successfully to the spherical wrist and was lightweight enough to be quickly reoriented. The actuator interfaced properly with a *da Vinci* disposable faceplate, allowing surgical tools to be easily and reliably mounted to the module. One element the design team did not successfully implement was the positional control of the actuator module's 4 DC motors. Although the control system was designed, due to hardware lead times and project timing, the actuator module was left unpowered during final demonstrations. This shortcoming did not inhibit the design team's ability to confirm the functionality of the rest of the system.

Perhaps one of the most influential contributions this project has brought to haptics research and telesurgery is the force sensing module. This module seamlessly integrates between a *da Vinci* arm and surgical tool, without modification to either device. Since custom force sensing elements were developed to externally capture joint torques, the sensing module does not inhibit the *da Vinci's* functionality. The module's low profile and relatively slim packaging are testament to its requirements of not interfering with the surgical workspace. Of all subcomponents, the design team believes this module may have the greatest potential to influence future research.

The sensor elements are highly reliable. Torques within the specified operational range were measured precisely. Perhaps the most important thing to note is that with simple manufacturing and assembly, these well-designed sensors show promising performance, easily capturing joint torques. However, with slight improvements in manufacturing and the quality of strain gage elements, these sensors could see even further success and be applied in a multitude of applications requiring direct torque measurement.

The Linux-based control system developed for this project shows that real-time control of a robotic platform is complex but very possible to do with readily available components. Although the organization and integration of the control system's components was unique, the components themselves are inexpensively available. The design team found it difficult to configure the Linux Kernel with the RTAI patch, however this may be attributed to the team's inexperience with the Linux operating system prior to this project. The development of this real-time system will enable future telesurgery research at WPI.

The haptic interface enables forces to be easily applied to the operator's hand. Although the design team's chosen interface, the Novint Falcon, is only capable of applying forces in three dimensions, research indicates that for some surgical maneuvers this may be sufficient (Verner and Okamura). Also, the simplification of the haptic interface reduces cost considerably, with the cost of a Falcon device currently under $200. The interface is at least a starting point for the haptics research platform and can be easily exchanged with another commercially available system or custom device.

8. FUTURE WORK

There are several elements the team envisions in terms of future work. The first is user evaluation. Using the robotic *da Vinci* simulator, evaluations should be performed assessing an individual's ability to interpret tool-tissue interaction forces. This will help determine which tool-interaction forces are important and worth feeding back to the user via the haptic device. Such questions as: What sensitivity in tool interaction forces is necessary to distinguish between common tissue types? What mapping of tool-interaction forces to Cartesian haptic forces is most effective for the user to interpret the internal environment of a simulated patient? And, how can the user or an algorithm effectively control and optimize the amount and timing of haptic feedback to increase procedural efficient? are important for future research.

Furthermore, the research team believes it would be worthwhile to investigate how latency between user input/feedback and robot motion affect a procedure. What is a tolerable amount of delay in real-time surgery and how can unacceptable delays be compensated for in remote telesurgery. This field is in its infancy and such work would provide necessary information to researchers.

The team envisions a more robust and stable robot. Mechanical stabilization of the wrist, motor module, and actuator module should be considered. Given the time constrains of the project, the team had virtually no time to optimize and further redesign mechanical components.

Lastly, a clinically viable solution would benefit surgeons and other medical practitioners. If this single *da Vinci* arm could be used in a clinical scenario, it may add flexibility to robot-assisted procedures. Perhaps more feasibly, the robotic platform could assist in the training of practitioners. Logging time on a multimillion dollar system that is rarely available can increase the learning curve of robot-assisted surgery. However, if an independent system can be utilized to train practitioners, the system could potentially decrease the time it takes a surgeon to become proficient at robot-assisted surgery.

REFERENCES

1. Berkelman, Peter and Ji Ma. "A Compact Modular Teleoperated Robotic System for Laparoscopic Surgery." The International Journal of Robotics Research 28 (2009): 1198–1215.
2. Elhage, Oussama, et al. "Robotic Urology in the United Kingdom: Experience and Overview." J Robotic Surg 1 (2008): 235–242.
3. Feller, R L, et al. "The Effect of Force Feedback on Remote Palpation." IEEE International Conference on Robotics and Automation. New Orleans, 2004.
4. Haidegger, Tamas, et al. "Force Sensing and Force Control for Surgical Robots." Proceedings of the 7th IFAC Symposium on Modelling and Control in Biomedical Systems. Aalborg, Denmark: IFAC, 2009.
5. Intuitive Surgical. Intuitive Surgical - Products. 2010. 25 4 2010 <http://www.intuitivesurgical.com/products/index.aspx>.
6. Ishii, Chiharu, et al. "Robotic Forceps Manipulator With a Novel Bending Mechanism." IEEE/ASME TRANSACTIONS ON MECHATRONICS (2010).
7. Lenihan, John P, Carol Kovanda and Usha Seshadri-Kreaden. "What is the Learning Curve for Robotic Assisted Gynecologic Surgery?" Journal of Minimally Invasive Gynecology 15 (2008): 589-594.
8. Lum, Mitchell J H, et al. "The RAVEN: Design and Validation of a Telesurgical System." The International Journal of Robotics Research 28 (2009): 1183–1197.
9. Mahvash, M and A Okamura. "Friction Compensation for Enhancing Transparency of a Teleoperator with Compliant Transmission." IEEE Transactions on Robotics 23 (2007): 1240-1246.
10. Mottrie, Alexandre M. "The Introduction of Robot-Assisted Surgery in Urologic Practice: Why Is It So Difficult?" European Urology 57 (2010): 747-749.
11. Okamura, A M. "Methods for Haptic Feedback in Teleoperated Robot-Assisted Surgery." Industrial Robot: An International Journal 31 (2004): 499–508.
12. Scales, Charles D, et al. "Local Cost Structures and the Economics of Robot Assisted Radical Prostatectomy." The Journal of Urology 174 (2005): 2323–2329.
13. Spong, Mark W, Seth Hutchinson and Vidyasagar M. Robot Dynamics and Control. Wiley, 1989.
14. Sun, L W, et al. "Advanced da Vinci surgical system simulator for surgeon training and operation planning." Int J Med Robotics Comput Assist Surg 3 (2007): 245–251.
15. Trejos, A L, et al. "Robot-assisted Tactile Sensing for Minimally Invasive Tumor Localization." The International Journal of Robotics Research 28 (2009): 1118-1133.

16. Verner, Lawton N and Allison M Okamura. "Force & Torque Feedback vs Force Only Feedback." Third Joint Eurohaptics Conference and Symposium on Haptic Interfaces for Virtual Environment and Teleoperator Systems. Salt Lake City: IEEE, 2009.